bioRxiv preprint doi: https://doi.org/10.1101/2021.11.18.469088; this version posted November 18, 2021. The copyright holder for this preprint (which was not certified by peer review) is the author/funder. All rights reserved. No reuse allowed without permission.

Structural basis for Cas9 off-target activity

Martin Pacesa[1], Chun-Han Lin[2,3], Antoine Cléry[4], Katja Bargsten[1,5], Matthew J. Irby[2], Frédéric H.T. Allain[4], Peter Cameron[2,6], Paul D. Donohoue[2], Martin Jinek[1]

Address:

[1]Department of Biochemistry, University of Zurich, Winterthurerstrasse 190, CH-8057 Zurich, Switzerland

[2]Caribou Biosciences, 2929 Seventh Street #105, Berkeley, CA 94710, United States

[3]Present address: LinkedIn, Sunnyvale, CA 94085, United States

[4]Institute of Biochemistry, ETH Zurich, Hönggerbergring 64, CH-8093 Zurich, Switzerland

[5]Present address: leadXpro AG, Villigen, Switzerland

[6]Present address: Spotlight Therapeutics, Hayward, CA 94545, United States

Corresponding author: Martin Jinek (jinek@bioc.uzh.ch)

bioRxiv preprint doi: https://doi.org/10.1101/2021.11.18.469088; this version posted November 18, 2021. The copyright holder for this preprint (which was not certified by peer review) is the author/funder. All rights reserved. No reuse allowed without permission.

Abstract

The target DNA specificity of the CRISPR-associated genome editor nuclease Cas9 is determined by complementarity to a 20-nucleotide segment in its guide RNA. However, Cas9 can bind and cleave partially complementary off-target sequences, which raises safety concerns for its use in clinical applications. Here we report crystallographic structures of Cas9 bound to *bona fide* off-target substrates, revealing that off-target binding is enabled by a range of non-canonical base pairing interactions and preservation of base stacking within the guide–off-target heteroduplex. Off-target sites containing single-nucleotide deletions relative to the guide RNA are accommodated by base skipping rather than RNA bulge formation. Additionally, PAM-distal mismatches result in duplex unpairing and induce a conformational change of the Cas9 REC lobe that perturbs its conformational activation. Together, these insights provide a structural rationale for the off-target activity of Cas9 and contribute to the improved rational design of guide RNAs and off-target prediction algorithms.

bioRxiv preprint doi: https://doi.org/10.1101/2021.11.18.469088; this version posted November 18, 2021. The copyright holder for this preprint (which was not certified by peer review) is the author/funder. All rights reserved. No reuse allowed without permission.

Introduction

Cas9, the effector nuclease of prokaryotic Type II CRISPR adaptive immune systems (Makarova et al., 2020), cleaves double-stranded DNA substrates complementary to a guide CRISPR RNA (crRNA) (Jinek et al., 2012). By changing the sequence of the guide RNA, the target DNA specificity of the CRISPR-Cas9 system is readily programmable (Jinek et al., 2012), a feature that has been widely exploited for genome engineering applications (Anzalone et al., 2020). Cas9 functions in conjunction with a trans-activating crRNA (tracrRNA), which is required both for crRNA loading and subsequent DNA binding and cleavage (Deltcheva et al., 2011; Jinek et al., 2012). Target DNA binding and cleavage is further dependent on the presence of a protospacer-adjacent motif (PAM) flanking the target sequence (Anders et al., 2014; Jinek et al., 2012). Due to its high activity and 5'-NGG-3' PAM specificity, *Streptococcus pyogenes* Cas9 (SpCas9) remains the most widely used CRISPR-Cas nuclease for gene editing applications. However, despite a high intrinsic accuracy in generating targeted DNA breaks, SpCas9 can nevertheless cleave genomic DNA sequences with imperfect complementarity to the guide RNA, resulting in off-target editing (Cameron et al., 2017; Hsu et al., 2013; Pattanayak et al., 2013; Tsai et al., 2015). The off-target activity of SpCas9, as well as other Cas9 enzymes, thus presents a safety concern for their therapeutic applications.

Off-target sites typically contain one or several nucleobase mismatches relative to the guide RNA (Cameron et al., 2017; Tsai et al., 2017; Tsai et al., 2015). Recent studies have established that the type of mismatch, its positioning within the heteroduplex, and the total number of mismatches are important determinants of off-target DNA binding and cleavage (Boyle et al., 2017; Boyle et al., 2021; Doench et al., 2016; Jones et al., 2020; Zhang et al., 2020). PAM-proximal mismatches within the seed region of the guide RNA-target DNA strand heteroduplex typically have a dramatic impact on substrate DNA binding and R-loop formation (Boyle et al., 2021; Ivanov et al., 2020; Singh et al., 2016; Zhang et al., 2020). In contrast,

bioRxiv preprint doi: https://doi.org/10.1101/2021.11.18.469088; this version posted November 18, 2021. The copyright holder for this preprint (which was not certified by peer review) is the author/funder. All rights reserved. No reuse allowed without permission.

PAM-distal mismatches are compatible with stable binding; however, their presence often results in the formation of a catalytically incompetent complex (Boyle et al., 2021; Dagdas et al., 2017; Ivanov et al., 2020; Jones et al., 2020; Sternberg et al., 2015; Yang et al., 2018; Zhang et al., 2020). In addition, Cas9 has been shown to cleave off-target substrates containing insertions or deletions relative to the guide RNA sequence, which have been proposed to be recognized through the formation of nucleotide "bulges" in the guide RNA-target DNA heteroduplex (Boyle et al., 2021; Cameron et al., 2017; Doench et al., 2016; Jones et al., 2020; Lin et al., 2014; Tsai et al., 2015).

Numerous computational tools have been developed to predict possible genomic off-target sites based on sequence similarity (Bae et al., 2014; Stemmer et al., 2015). However, the majority of actual off-target cleavage events remain unpredicted (Cameron et al., 2017; Tsai et al., 2015). Furthermore, although Cas9 is able to bind genomic sites harbouring as few as five complementary nucleotides, only a relatively small number of off-target sites are actually cleaved and result in detectable off-target editing in cells (Kuscu et al., 2014; O'Geen et al., 2015; Wu et al., 2014). Several structures of target-bound Cas9 complexes have been determined to date (Anders et al., 2014; Jiang et al., 2016; Nishimasu et al., 2014; Zhu et al., 2019) that have shed light on the mechanism of on-target binding and cleavage. However, the same processes for off-target sites remain poorly understood.

To elucidate the mechanism of mismatch tolerance of Cas9, we determined crystal structures of a comprehensive set of *bona fide* off-target–bound complexes. These structures reveal that the formation of non-canonical base pairs and preservation of heteroduplex shape underpin the off-target tolerance of Cas9. We also observe that consecutive mismatches in the seed region can be accommodated by base skipping of a guide RNA nucleotide, as opposed to nucleotide bulging. Finally, the structure of an off-target complex containing three PAM-distal mismatches exhibits REC2/3 domain rearrangements, which likely perturbs conformational

bioRxiv preprint doi: https://doi.org/10.1101/2021.11.18.469088; this version posted November 18, 2021. The copyright holder for this preprint (which was not certified by peer review) is the author/funder. All rights reserved. No reuse allowed without permission.

activation of Cas9 and thus modulates cleavage efficiency. Taken together, our structural data reveal the diversity of mechanisms enabling off-target recognition and lay the foundation for engineering optimized CRISPR-Cas9 complex designs for gene editing.

bioRxiv preprint doi: https://doi.org/10.1101/2021.11.18.469088; this version posted November 18, 2021. The copyright holder for this preprint (which was not certified by peer review) is the author/funder. All rights reserved. No reuse allowed without permission.

Results

In vitro profiling reveals diversity of Cas9 off-targets

Multiple studies have investigated the off-target activity of Cas9, suggesting context-dependent tolerance of nucleobase mismatches between the guide RNA and off-target DNA sequences (Boyle et al., 2021; Cameron et al., 2017; Lazzarotto et al., 2020; Tsai et al., 2015; Zhang et al., 2020). To investigate the effect of mismatches on Cas9 binding and cleavage, we performed the SITE-Seq® assay (Cameron et al., 2017) to define the off-target landscapes of 12 well-studied guide RNAs to select suitable off-targets for further evaluation (**Table S1, Table S2**) (**Figure S1A-B**). The SITE-Seq assay analysis revealed a total of 3,848 detectable off-target sites at the highest Cas9 ribonucleoprotein (RNP) concentration, with a total of 21,732 base mismatches and a median of 5 mismatches per off-target site (**Figure S1C**). The detected mismatches covered all possible base mismatch combinations and were distributed throughout the length of the guide RNA-target DNA heteroduplex (**Figure S1D-E**).

To probe the thermodynamics of on- and off-target substrate DNA binding and the kinetics of DNA cleavage, we focused on a subset of four guide RNAs (*AAVS1*, *FANCF*, *PTPRC-tgt2,* and *TRAC*) and a total of 15 *bona fide* off-target sites detectable *in vivo* (Cameron et al., 2017; Donohoue et al., 2021; Tsai et al., 2017; Tsai et al., 2015) (**Figure 1A**) that covered all 12 possible base mismatch types. Nuclease activity assays using synthetic DNA substrates with fluorophore-labeled target strand (TS) revealed that all selected off-target sequences were cleaved slower than the corresponding on-target substrates, with 20–500-fold reductions in the calculated rate constants (**Figure 1B, Figure S2A**). To distinguish whether the cleavage defects were due to slower R-loop formation or perturbations in downstream steps, including conformational activation of the nuclease domains, we also quantified cleavage kinetics using PAMmer DNA substrates (Anders et al., 2014; O'Connell et al., 2014) in which the on-/off-target sequence was single-stranded. These experiments revealed that the slower cleavage

bioRxiv preprint doi: https://doi.org/10.1101/2021.11.18.469088; this version posted November 18, 2021. The copyright holder for this preprint (which was not certified by peer review) is the author/funder. All rights reserved. No reuse allowed without permission.

kinetics of most off-target substrates was due to perturbed R-loop formation (**Figure 1B, Figure S2B**). However, for some off-targets, notably *AAVS1* off-targets #2 and #5, *FANCF* off-targets #3, #4, and #6, and *PTPRC-tgt2* off-target #1, the rate of PAMmer substrate cleavage was more than 100-fold slower as compared to their respective on-target sequences (**Figure 1B**, **Figure S2B**). This indicates that these off-target mismatches may additionally cause perturbations in the conformational activation checkpoint downstream of guide-target hybridization or inhibit cleavage by direct steric hindrance of the Cas9 HNH domain (Chen et al., 2017; Dagdas et al., 2017).

Complementary quantification of substrate DNA binding using DNA nanolever (switchSENSE) methodology revealed perturbations in binding affinities for most off-targets as compared to the respective on-target sequences (**Figure 1B, Data S1**). Notably, the reductions in binding affinities were almost entirely due to increased dissociation rates (k_{off}), while on-binding rates (k_{on}) were largely unperturbed (**Figure 1B**), indicating that most of the off-target mismatches in our data set promote DNA dissociation, likely due to R-loop collapse. However, there was little correlation between the observed reductions in cleavage rates and binding constants (**Figure S2C**), confirming that the molecular basis for off-target discrimination by Cas9 is not based on substrate binding alone, in agreement with prior studies (Boyle et al., 2021; Chen et al., 2017; Dagdas et al., 2017; Jones et al., 2020; Yang et al., 2018; Zhang et al., 2020). The dissociation rate (k_{off}) correlated significantly only with the number of mismatches located in the seed region (R^2=0.46, p=0.001) (**Figure S2C**), suggesting that off-targets with mismatches in the seed are regulated mainly through R-loop collapse and non-target strand (NTS) rehybridization (Boyle et al., 2017; Gong et al., 2018; Singh et al., 2016; Sternberg et al., 2014).

Finally, we correlated the measured cleavage rate constants (k_{obs}) with predicted data based on a leading biophysical model of Cas9 off-target cleavage that accounts for mismatch

bioRxiv preprint doi: https://doi.org/10.1101/2021.11.18.469088; this version posted November 18, 2021. The copyright holder for this preprint (which was not certified by peer review) is the author/funder. All rights reserved. No reuse allowed without permission.

number and position using position-dependent penalties and includes position-independent weights for mismatch type (Jones et al., 2020). Although there was good overall correlation between the model and our data (R^2=0.46, p=0.004) (**Figure S2C**), there were nevertheless several prominent outliers (*AAVS1* off-target #2 and off-target #3, and *FANCF* off-target #4), suggesting that accurate modelling of off-target interactions will require accounting for position-specific effects of individual mismatch types (**Figure S2D**).

Taken together, these results indicate that *bona fide* off-target substrates exhibit significantly perturbed kinetics of substrate DNA binding and cleavage. Moreover, the magnitude of the perturbation is dependent not only on the number and position of mismatches in the off-target sequence but also on mismatch type, in agreement with recent studies (Boyle et al., 2021; Doench et al., 2016; Jones et al., 2020; Zhang et al., 2020). Moreover, the off-target activity cannot be accurately predicted by biophysical off-target activity models that account for mismatch type in a position-independent manner, implying that mismatches have position-specific and context-dependent effects. This further highlights the need to understand the molecular principles of Cas9 off-target recognition at the structural level.

Crystallographic analysis of off-target interactions

To obtain insights into the structural basis of off-target recognition and mismatch tolerance, we employed a previously described approach (Anders et al., 2014) to co-crystallize Cas9 with sgRNA guides and partially duplexed off-target DNA substrates (**Figure 1C**). Focusing on our set of *AAVS1*, *FANCF*, *PTPRC-tgt2* and *TRAC* off-targets (**Figure 1A**), covering all 12 possible mismatch types, we determined a total of 15 off-target complex structures at resolutions of 2.25–3.30 Å (**Figure 1C**, **Table S3)**. For the *AAVS1*, *FANCF* and *TRAC* guide RNAs, we also determined the structures of the corresponding on-target complexes; the structure of the *PTPRC-tgt2* on-target complex could not be determined due to insufficient diffraction of the crystals. Overall, the off-target complex structures have very similar conformations, with the

bioRxiv preprint doi: https://doi.org/10.1101/2021.11.18.469088; this version posted November 18, 2021. The copyright holder for this preprint (which was not certified by peer review) is the author/funder. All rights reserved. No reuse allowed without permission.

Cas9 polypeptide backbone superimposing with a mean root mean square deviation of 0.41Å over 1330 Cα atoms (as referenced to the *FANCF* on-target complex structure, excluding *FANCF* off-target #4, as discussed below). Of note, the *AAVS1* on-target complex structure reveals substantial repositioning of the REC2 domain, where it undergoes a 12° rotation (as compared to the *FANCF* and *TRAC* on-target complexes) (**Figure S3A**), with concomitant shortening of the α-helix comprising residues 301-305 and restructuring of the loop comprising residues 175-179 (**Figure S3B**), enabled by the absence of crystal contacts involving the REC2 and REC3 domains.

However, the structures display considerable local variation of the RNA-TS DNA heteroduplex conformation. Base base pairing and base stacking are mostly preserved throughout the guide RNA-TS DNA heteroduplexes (**Table S4**), with the exception of positions 1–3 within the PAM-distal end of the guide-TS duplex, where the presence of mismatches results in duplex unpairing. This is observed in *AAVS1* off-target #2 and #4, *FANCF* off-target #4 and #5, and *TRAC* off-target #1 complexes (**Figure S4**). Despite the observed conformational variation, the off-target structures preserve almost all intermolecular contacts between the Cas9 protein and the bound nucleic acids, further underscoring the structural plasticity of Cas9 in accommodating mismatch-induced distortions in the guide RNA-TS DNA heteroduplex.

Together, these observations indicate that the crystal form used for determination of the off-target complex structures is sufficiently plastic to accommodate conformational changes resulting from the presence of base mismatches in the guide RNA–TS DNA heteroduplex and imply that the observed structural effects of guide RNA–TS DNA base mismatches provide a true depiction of off-target DNA binding. In addition, the HNH and REC2/3 domain conformations observed in the crystal structures are similar to those observed in the 16-bp heteroduplex, pre-checkpoint state determined by cryo-EM (Pacesa and Jinek, 2021).

bioRxiv preprint doi: https://doi.org/10.1101/2021.11.18.469088; this version posted November 18, 2021. The copyright holder for this preprint (which was not certified by peer review) is the author/funder. All rights reserved. No reuse allowed without permission.

Non-canonical base-pairing interactions facilitate off-target recognition

Close inspection of the 15 Cas9 off-target complex structures reveals that a substantial fraction of off-target base mismatches (34 out of 49) is accommodated by non-canonical base pairing interactions that preserve at least one hydrogen bond between the guide and off-target bases. The most common off-target mismatches, both in our data set (**Table S1, Table S2**) and as reported by other studies (Boyle et al., 2017; Doench et al., 2016; Hsu et al., 2013; Jones et al., 2020; Pattanayak et al., 2013; Zhang et al., 2020), are rG-dT (**Figure S5**) and rU-dG (**Figure 2A, Figure S6**), which have the potential to form wobble base pairs (Kimsey et al., 2015). Indeed, all rG-dT mismatches in the determined structures are accommodated by wobble base pairing. At duplex positions 4 (*AAVS1* off-target #1 and #5), 13 (*FANCF* off-target #2 and #7) and 15 (*TRAC* off-target #1), the dT base undergoes a ~1 Å shear displacement into the major groove of the guide–TS DNA heteroduplex to form the wobble base pair (**Figure S5**), whereas at duplex position 2 (in *TRAC* off-target #1 and #2), wobble base pairing is enabled by a minor groove displacement of the rG base. In contrast, rU-dG mispairs in the determined structures exhibit considerable structural variation. At duplex position 10 in the *FANCF* off-target #2 and #4 complexes, the rU base is able to undergo the major groove displacement required for wobble base-pairing (**Figure 2A, Figure S6A**). In contrast, at duplex position 5 in *FANCF* off-target #1, #3 and #6 complexes, the backbone of the RNA strand makes extensive contacts with Cas9 (**Figure S6B-D**). As a result, the rU-dG mispairs are instead accommodated by compensatory shifts of the dG base to maintain hydrogen-bonding interactions (**Figure S6B-D**). At duplex position 9 in the *TRAC* off-target #1 complex, the rU-dG mismatch is accommodated by wobble base-pairing enabled by a minor groove displacement of the dG base (**Figure S6E**). At the same duplex position in the *AAVS1* off-target #1 and #2 complexes, however, this mispair occurs next to rC-dA and rC-dT mismatches, respectively, and adopts the sterically prohibited Watson-Crick geometry (**Figure S6F-G**), implying a tautomeric shift or

bioRxiv preprint doi: https://doi.org/10.1101/2021.11.18.469088; this version posted November 18, 2021. The copyright holder for this preprint (which was not certified by peer review) is the author/funder. All rights reserved. No reuse allowed without permission.

base deprotonation to accommodate this otherwise unfavorable base pairing mode (**Figure S6H**). Collectively, these observations suggest that the ability of rU-dG (and likely rG-dT) mismatches to form wobble base pairing interactions is determined not only by backbone constraints at the specific position within the guide RNA-TS DNA heteroduplex, but also by local sequence context and/or the presence of neighboring mismatches.

rA-dC or rC-dA mismatches can also form wobble-like base pairs when the adenine base is protonated at the N1 position (Garg and Heinemann, 2018; Wang et al., 2011). In the rA-dC mispairs found at duplex position 4 in the *FANCF* off-target #2 and #3 complexes, the dC nucleotide undergoes a wobble displacement compatible with the formation of two hydrogen bonds with adenine base, indicative of adenine protonation (**Figure 2B**, **Figure S7A**). At other duplex positions in our data set, the rA-dC or rC-dA mispairs are instead accommodated by slight displacements of the adenine base within the base pair plane resulting in the formation of a single hydrogen bond in each case (**Figure S7B-D**).

Accommodating purine-purine mismatches by Watson-Crick-like interactions would normally require severe distortion of the guide–off-target duplex to increase its width by more than 2 Å (Leontis et al., 2002). At positions where the duplex width is constrained by Cas9 interactions, rG-dA and rA-dG mispairs are accommodated by *anti*-to-*syn* isomerization of the adenine base to form two hydrogen-bonding interactions via its Hoogsteen base edge. This is observed at duplex position 11 in the *AAVS1* off-target #4 complex (rG-dA mispair) (**Figure 2C**) and at position 7 in the *AAVS1* off-target #2 complex (rA-dG mispair) (**Figure S7E**). Similarly, the rG-dG mispair at duplex position 13 in the *FANCF* off-target #5 complex is accommodated by Hoogsteen base-pairing as a result by *anti*-to-*syn* isomerization of the guide RNA base (**Figure 2D**). Overall, the observed Hoogsteen base pairing interactions are near-isosteric with Watson-Crick base pairs and maintain duplex width without excessive backbone distortion (**Table S4**).

bioRxiv preprint doi: https://doi.org/10.1101/2021.11.18.469088; this version posted November 18, 2021. The copyright holder for this preprint (which was not certified by peer review) is the author/funder. All rights reserved. No reuse allowed without permission.

Taken together, the prevalence of non-canonical base-pairing interactions, such as wobble and Hoogsteen base pairing, in off-target structures indicates that they serve a fundamental role in off-target recognition. These interactions preserve hydrogen bonding between guide RNA and off-target DNA bases while simultaneously maintaining the integrity of the guide RNA–off-target DNA heteroduplex and minimizing its structural distortions.

Duplex backbone rearrangements accommodate otherwise non-permissive base mispairs

Whereas wobble (G-U/T or A-C) and Hoogsteen (A-G or G-G) base pairs are generally compatible with the canonical A-form geometry of an RNA-DNA duplex, other nucleotide mismatches only form non-isosteric base pairs that require considerable distortion of the (deoxy)ribose-phosphate backbone. The formation of pyrimidine-pyrimidine base pairs is expected to occur by a substantial reduction in duplex width. This is observed at the rU-dC mismatch at duplex position 9 in the *FANCF* off-target #1 complex (**Figure 3A**). Here, the guide RNA backbone is able to shift towards the target DNA strand, resulting in a reduction of the C1'–C1' distance to 8.65 Å as compared to 10.0 Å in the *FANCF* on-target complex. This facilitates the formation of two hydrogen bonding interactions within the rU-dC base pair, which is further enabled by a substantial increase in base propeller twist (**Figure 3A**). In contrast, rC-dT mismatches remain unpaired at duplex positions 6 and 7 in *FANCF* off-target #6 and #7 complexes (**Figure S8A-B**), respectively, or form only a single hydrogen bond at position 8 in the *AAVS1* off-target #2 complex (**Figure S8C**), likely due to backbone steric constraints at these positions imposed by Cas9 interactions. Of note, the *FANCF* off-target #7 rC-dT mispair is bridged by hydrogen bonding interactions with the side chain of Arg895 inserted into the minor groove of the heteroduplex (**Figure S8B**); however, the interaction is not essential for the tolerance of rC-dT mismatches at this position (**Figure S9**). Backbone steric constraints also likely influence the formation of rU-dT base pairs. At duplex position 7 in the *TRAC* off-target #2 complex, the mismatch remains unpaired (**Figure S8D**), whereas

bioRxiv preprint doi: https://doi.org/10.1101/2021.11.18.469088; this version posted November 18, 2021. The copyright holder for this preprint (which was not certified by peer review) is the author/funder. All rights reserved. No reuse allowed without permission.

productive pairing is seen at duplex positions 8 (*PTPRC-tgt2* off-target #1 complex) and 9 (*FANCF* off-target #5 and *TRAC* off-target #2 complexes), facilitated by distortions of the guide RNA and TS backbone, respectively (**Figure 3B, Figure S8E-F**).

rC-dC mispairs only form productive hydrogen-bonding interactions if bridged by a water molecule or when one of the cytosine bases is protonated (Leontis et al., 2002). Only the former is observed in the determined structures, at duplex position 5 in the *AAVS1* off-target #2 complex (**Figure S8G**). In contrast, at duplex position 8 and 15 in the *AAVS1* off-target #3 complex, the bases remain unpaired while maintaining intra-strand base stacking interactions (**Figure 3C, Figure S8H**). Similarly, rA-dA mispairs are unable to form productive hydrogen-bonding interactions within the constraints of an A-form duplex (Leontis et al., 2002). Accordingly, the rA-dA mispair at duplex position 5 in the *PTPRC-tgt2* off-target #1 complex is accommodated by extrusion of the dA nucleobase out of the base stack into the major groove of the duplex (**Figure 3D**). As the duplex width is constrained at this position by Cas9, the base extrusion is enabled by local distortion of the TS backbone (**Figure S10A**). Analysis of our SITE-Seq assay data set revealed that off-target rA-dA mispairs occur at all positions within the guide RNA–TS DNA heteroduplex (**Figure S10B**), in agreement with previous studies (Boyle et al., 2017; Boyle et al., 2021; Doench et al., 2016; Jones et al., 2020; Zhang et al., 2020). This suggests that rA-dA mismatches do not encounter steric barriers within Cas9 that would disfavour their presence, which is consistent with the absence of specific contacts with Cas9 along the length of the major groove of the guide RNA–TS DNA duplex.

Collectively, these structural findings indicate that conformational rearrangements of the (deoxy)ribose-phosphate backbone of the guide RNA or TS DNA facilitate interactions of base mispairs that would otherwise be incompatible with canonical A-form duplex geometry. The specific mechanism of base mismatch accommodation at a given position is governed by

bioRxiv preprint doi: https://doi.org/10.1101/2021.11.18.469088; this version posted November 18, 2021. The copyright holder for this preprint (which was not certified by peer review) is the author/funder. All rights reserved. No reuse allowed without permission.

local steric constraints on duplex width and the ability of the guide RNA or TS DNA to undergo backbone distortions, which are in turn dictated by local interactions with Cas9.

PAM-proximal mismatches are accommodated by TS distortion due to seed sequence rigidity

The seed sequence of the guide RNA (nucleotides 11-20) makes extensive interactions with Cas9, both in the absence and presence of bound DNA (Anders et al., 2014; Jiang et al., 2015; Nishimasu et al., 2014; Zhu et al., 2019). Structural pre-ordering of the seed sequence by Cas9 facilitates target DNA binding and contributes to the specificity of on-target DNA recognition (Jiang et al., 2015; O'Geen et al., 2015; Wu et al., 2014). Conversely, binding of off-target DNAs containing PAM-proximal mismatches is inhibited and results in accelerated off-target dissociation (Boyle et al., 2017; Boyle et al., 2021; Ivanov et al., 2020; Jones et al., 2020; Singh et al., 2016; Zhang et al., 2020). Nevertheless, Cas9 does tolerate most base mismatch types within the seed region of the guide RNA, leading to detectable off-target DNA cleavage (Boyle et al., 2021; Doench et al., 2016; Jones et al., 2020; Zhang et al., 2020). In particular, the first two PAM-proximal positions display a markedly higher tolerance for mismatches than the rest of the seed region (Cofsky et al., 2021; Doench et al., 2016; Hsu et al., 2013; Mekler et al., 2017; Zeng et al., 2018); this is supported by our SITE-Seq assay data as the frequency of mismatches at the first three PAM-proximal positions is roughly twice as high as at the other seed sequence positions (**Figure S1D-E**).

Unlike the seed region of the guide RNA, the complementary PAM-proximal TS nucleotides are not directly contacted by Cas9 in the pre-cleavage state and are thus under fewer steric constraints, with the exception of duplex position 20 in which the phosphodiester group of the TS nucleotide makes extensive interactions with the phosphate lock loop of Cas9 (Anders et al., 2014) (**Figure S11A**). In agreement with this, our off-target complex structures reveal that PAM-proximal base mismatches are accommodated solely by structural distortions of the

bioRxiv preprint doi: https://doi.org/10.1101/2021.11.18.469088; this version posted November 18, 2021. The copyright holder for this preprint (which was not certified by peer review) is the author/funder. All rights reserved. No reuse allowed without permission.

TS backbone, while the conformation of the guide RNA backbone and base stacking within the seed region remain unperturbed. The presence of an rA-dA mismatch in the PAM-proximal position 18 of *FANCF* off-target #6 results in the extrusion of the TS nucleobase into the major groove (**Figure 4A**), likely due to steric constraints on duplex width at this position. In contrast, the rA-dA mismatch at duplex position 19 in the *AAVS1* off-target #2 is instead accommodated by a marked distortion in the TS backbone that results in increased duplex width, which preserves base stacking within the duplex in the absence of productive pairing between the adenine bases (**Figure 4B**, **Figure S11B**). Similarly, the rA-dG mismatch at position 19 in the *AAVS1* off-target #5 is accommodated by a ~2 Å displacement of the TS backbone, increasing duplex width. This not only preserves base stacking but also facilitates rA-dG base paring by two hydrogen bonding interactions via their Watson-Crick edges (**Figure 4D**, **Figure S11C**). This off-target complex also contains a rU-dG mispair at duplex position 20 which does not undergo wobble base pairing as the rU20 nucleotide is extensively contacted by Cas9 and unable to shift towards the major groove and is instead accommodated by a slight shift in the dG nucleotide (**Figure 4D**). Finally, the rU-dT base mismatch at duplex position 20 in the *AAVS1* off-target #4 complex remains unpaired and the dT base lacks ordered electron density (**Figure 4C**). This is likely a result of the dT nucleotide maintaining contact with the phosphate-lock loop of Cas9, which prevents a reduction in the duplex width and precludes productive base pairing.

Overall, these observations indicate that off-target DNAs containing mismatches to the seed sequence of the guide RNA can be accommodated by Cas9 due to limited interactions with the TS DNA in the seed-binding region, which permits structural distortions of the TS backbone to accommodate base mispairs without steric hindrance and may facilitate non-canonical base pairing interactions. Conversely, the extensive interactions of Cas9 with the ribose-phosphate

bioRxiv preprint doi: https://doi.org/10.1101/2021.11.18.469088; this version posted November 18, 2021. The copyright holder for this preprint (which was not certified by peer review) is the author/funder. All rights reserved. No reuse allowed without permission.

backbone of the seed region of the guide RNA provide strong steric constraints that would be expected to disfavour specific base mispairs.

Cas9 recognizes off-targets with single-nucleotide deletions by base skipping or via multiple mismatches

A substantial fraction of *bona fide* off-target sites recovered in our SITE-Seq assay analysis (46.4%, when not considering the possibility of nucleotide insertions or deletions) contained six or more mismatched bases to the guide RNA (**Figure S1C**, **Table S1, Table S2**). Such off-target sequences have previously been proposed to be accommodated by bulging out or skipping of nucleotides (Boyle et al., 2021; Cameron et al., 2017; Doench et al., 2016; Jones et al., 2020; Lin et al., 2014; Tsai et al., 2015), which would result in a shift of the nucleotide register to re-establish correct base pairing downstream of the initially encountered mismatch. The *PTPRC-tgt2* off-target #1, *FANCF* off-target #3 and *AAVS1* off-target #2 sites are predicted to contain single nucleotide deletions at duplex positions 15, 17 and 9, respectively (**Figure 1A**, **Figure 5C**). Structures of the *PTPRC-tgt2* off-target #1 and *FANCF* off-target #3 complexes reveal that the single nucleotide deletions in these off-target substrates are not accommodated by bulging out the unpaired guide RNA nucleotide. Instead, the conformations of the guide RNAs remain largely unperturbed and the off-target TS DNAs "skip over" the unpaired RNA bases to resume productive base-pairing downstream (**Figure 5A-B**). Comparisons with the *FANCF* on-target complex structure show that the seed sequences of the guide RNAs are held in place by interactions with the bridge helix and the REC1 domain, whereas the DNA target strand phosphate backbones are displaced by almost 3 Å (**Figure S12A-B**). The base pair skips are accommodated by considerable buckling and tilting of the base pairs immediately downstream of the skip site. An additional consequence of the base pairing register shift is the formation of non-canonical base pairs between the off-target DNA and the extra 5'-terminal guanine nucleotides present in the guide RNA as a consequence of *in vitro* transcription by T7

bioRxiv preprint doi: https://doi.org/10.1101/2021.11.18.469088; this version posted November 18, 2021. The copyright holder for this preprint (which was not certified by peer review) is the author/funder. All rights reserved. No reuse allowed without permission.

RNA polymerase (**Figure S12C-D**). This potentially explains the impact of the 5'-guanines on both R-loop stability and *in vitro* cleavage activity (Kulcsar et al., 2020; Mullally et al., 2020; Okafor et al., 2019).

Originally, our SITE-Seq assay analysis annotated the *AAVS1* off-target #2 as a single-nucleotide deletion at duplex position 9 (**Figure 5C**). Unexpectedly, the structure of the *AAVS1* off-target #2 complex instead reveals that the off-target substrate is bound in the unshifted register, resulting in the formation of five base mismatches in the PAM-distal half of the guide RNA–TS duplex (**Figure 5D**), including a partially paired rC-dC mismatch at position 5, an rA-dG Hoogsteen pair at position 7, a partially paired rC-dT mismatch at position 8, and a tautomeric rU-dG pair at position 9. The backbone conformations of the guide RNA and the off-target TS exhibit minimal distortions and are nearly identical with the corresponding on-target heteroduplex (**Figure 5D**), suggesting an explanation for the tolerance of the multiple mismatches in this off-target site, and implying that certain mismatch combinations might cumulatively result in guide RNA and TS backbone conformations that mimic the on-target situation. To test this hypothesis, we reverted the rC-dT mismatch at position 8 to the on-target rC-dG pair, thereby reducing the total amount of off-target mismatches from 6 to 5 (**Figure 5C**). The resulting off-target substrate (*AAVS1* off-target #6) exhibited substantially reduced cleavage rates in both dsDNA and PAMmer formats, as well as a significantly increased dissociation rate (**Figure 5E-F**). These results suggest that for some *bona fide* off-target substrates containing mismatch combinations, the reversal of one mismatch may affect the structural integrity of the guide RNA–TS DNA heteroduplex and interfere with DNA binding and/or conformational activation of Cas9, despite a reduction in the total number of mismatches.

Collectively, these results indicate that deletion-containing off-target complexes are accommodated either by RNA base skipping, as opposed to RNA nucleotide bulging, or by the

bioRxiv preprint doi: https://doi.org/10.1101/2021.11.18.469088; this version posted November 18, 2021. The copyright holder for this preprint (which was not certified by peer review) is the author/funder. All rights reserved. No reuse allowed without permission.

formation of multiple base mismatches. The precise mechanism appears to be dependent on the position of the deletion. Because the seed sequence nucleotides 12-20 of the guide RNA are extensively contacted by Cas9 (**Figure S13**), while the complementary DNA nucleotides are able to undergo distortions to accommodate a shift in the base pairing register, deletions at positions within the PAM-proximal region of the guide RNA–TS heteroduplex (positions 11-20) result in RNA base skipping. In contrast, deletions at PAM-distal positions (1-10), where the guide RNA–TS DNA heteroduplex is constrained by interactions with the REC3 and HNH domains, are instead likely to be bound without a register shift via multiple mismatches.

In light of our structural findings, we computationally analyzed off-target sites identified by the SITE-Seq assay for the presence of insertions or deletions in the target DNA relative to the guide RNA sequence. Our initial off-target classification algorithm assumed that deletions and insertions can occur along the entire guide RNA–off-target DNA heteroduplex. Based on our structural data we subsequently constrained the algorithm to only consider single-nucleotide deletions and insertions at heteroduplex positions 10-20 and 6-20, respectively (**Figure S14**). This resulted in a substantial reduction in the number of off-targets containing deletions (from 323 to 277) but no change in off-targets predicted to contain insertions (116 sites for both). When extrapolated, these results collectively suggest that up to 14% of off-target sites previously annotated as containing deletions or insertions in off-target studies might instead be recognized via multiple mismatches (**Figure S15**), which has implications for off-target prediction, as discussed below.

PAM-distal mismatches perturb the Cas9 conformational checkpoint

FANCF off-target #4, which contains three PAM-distal mismatches at positions 1-3 and a G-U mismatch in position 10 (**Figure 1A**), is reproducibly the top ranking off-target site for the *FANCF* guide RNA, as detected by SITE-Seq assay analysis at the lowest Cas9 RNP concentrations (**Table S1, Table S2**). The off-target substrate exhibits slow cleavage kinetics

bioRxiv preprint doi: https://doi.org/10.1101/2021.11.18.469088; this version posted November 18, 2021. The copyright holder for this preprint (which was not certified by peer review) is the author/funder. All rights reserved. No reuse allowed without permission.

in vitro with both dsDNA and PAMmer substrates (**Figure 2B, Figure S2A-B**), indicating a perturbation of the conformational activation checkpoint of Cas9. The structure of the *FANCF* off-target #4 complex reveals that the RNA–DNA heteroduplex is unpaired at positions 1-3 as a result of the PAM-distal mismatches, with nucleotides 1-2 of the guide RNA and 19-20 of the TS disordered (**Figure 6A**). Furthermore, Cas9 undergoes structural rearrangements of its REC lobe and the HNH domain (**Figure 6B**), resulting in a root mean square displacement of the REC2 and REC3 domains of 3.7 Å (1,315 Cα atoms) relative to the *FANCF* on-target complex structure. The REC3 domain undergoes a 19-degree rotation (**Figure 6B**), facilitated by extending the helix comprising residues 703-712 through restructuring of loop residues 713-716 (**Figure S16A)**, to accommodate the altered guide RNA conformation. The REC2 domain rotates 32 degrees away from the REC3 domain (**Figure 6B**). This is accompanied by restructuring of the hinge loop residues 174-180 and disordering of loops 258-264, 284-285, and 307-309. Concomitantly, the HNH domain rotates 11^{o} away from the heteroduplex, as compared to the *FANCF* on-target structure, to accommodate distortion of the TS DNA (**Figure 6B**).

The unpaired 5' end of the sgRNA is located at the interface between the REC3 and the RuvC domain and maintains interactions with heteroduplex-sensing residues Lys510, Tyr515, and Arg661 of the REC3 domain **(Figure S16B).** In contrast to the corresponding on-target complex structure, the unpaired 3' end of the off-target TS breaks away from the REC3 lobe and instead points towards the REC2 domain, forming unique interactions with Arg895, Asn899, Arg905, Arg919 and His930 in the HNH domain (**Figure S16C**). These interactions **(Figure S16D)** could be responsible for the observed repositioning of the REC lobe and HNH domain, and they may impede the formation of a cleavage-competent complex.

The conformation of the *FANCF* off-target #4 complex is distinct from the conformations observed in cryo-EM reconstructions of the pre- and post-cleavage states of the

bioRxiv preprint doi: https://doi.org/10.1101/2021.11.18.469088; this version posted November 18, 2021. The copyright holder for this preprint (which was not certified by peer review) is the author/funder. All rights reserved. No reuse allowed without permission.

Cas9 complex (Zhu et al., 2019) (**Figure S17A-B**). Instead, the off-target complex structure most closely resembles that of a high-fidelity variant xCas9 3.7 containing amino acid substitutions that disrupt interactions with the TS DNA (Guo et al., 2019). Although the xCas9 3.7 complex adopts a slightly different REC lobe conformation (**Figure S17C**), the PAM-distal duplex also undergoes unpairing at positions 1–3 and displays a comparable degree of structural disorder (**Figure S17D**). These structural observations thus suggest that the presence of multiple mismatches in the PAM-distal region of a guide RNA–off-target DNA duplex leads to conformational perturbations in the DNA-bound complex that resemble the structural consequences of specificity-enhancing mutations in high-fidelity Cas9 variants.

bioRxiv preprint doi: https://doi.org/10.1101/2021.11.18.469088; this version posted November 18, 2021. The copyright holder for this preprint (which was not certified by peer review) is the author/funder. All rights reserved. No reuse allowed without permission.

Discussion

The off-target activity of Cas9 has been extensively documented in prior genome editing, biochemical and biophysical studies (Boyle et al., 2017; Boyle et al., 2021; Doench et al., 2016; Jones et al., 2020; Lazzarotto et al., 2020; Zhang et al., 2020). Although numerous methods have been devised for computational prediction of genomic off-target sites and their experimental validation, these have reported highly variable mismatch tolerance profiles depending on the screening method and the target sequence. Thus, a comprehensive understanding of this phenomenon is still lacking, particularly as to whether off-target tolerance has an underlying structural basis. In this study, we used the SITE-Seq assay to examine the off-target landscape of 12 well-studied guide RNAs, observing a broad variation of cleavage activities associated with individual off-target substrates. To shed light on the molecular mechanisms underpinning off-target activity, we determined atomic structures of a representative set of *bona fide* off-target complexes, thus providing fundamental insights into the structural aspects of off-target recognition.

Role of non-canonical base pairing in off-target recognition

The principal, and largely unexpected, finding of our structural analysis is that the majority of nucleotide mismatches in *bona fide* off-target substrates are accommodated by non-canonical base pairing interactions. These range from simple rG-dT/rU-dG wobble or Hoogsteen base pairing interactions, to pyrimidine-pyrimidine pairs that rely on (deoxy)ribose-phosphate backbone distortions that reduce duplex width. With the notable exception of rA-dA mispairs, which are accommodated at certain positions within the guide–TS heteroduplex by base extrusion, the structural rearrangements associated with base mismatch accommodation preserve base stacking, which is the primary determinant of nucleic acid duplex stability (Yakovchuk et al., 2006). For some off-target sequences, our structures are suggestive of base protonation or tautomerization, which facilitate hydrogen bonding interactions in otherwise

bioRxiv preprint doi: https://doi.org/10.1101/2021.11.18.469088; this version posted November 18, 2021. The copyright holder for this preprint (which was not certified by peer review) is the author/funder. All rights reserved. No reuse allowed without permission.

non-permissive base pair combinations, such as rA-dC. These rare base pair forms have been previously observed in both RNA and DNA duplexes and are thought to be important contributors to DNA replication and translation errors (Kimsey et al., 2015; Kimsey et al., 2018). Future studies employing complementary structural methods, such as nuclear magnetic resonance, will help confirm the occurrence of non-canonical base states in off-target complexes.

The mismatch tolerance of Cas9 can be explained primarily by two factors. Firstly, Cas9 does not directly contact the major- or minor-groove edges of the guide RNA–TS DNA heteroduplex base pairs at any of the duplex positions and thus lacks a steric mechanism to enforce Watson-Crick base pairing. This is further underscored by Cas9's tolerance of base modifications in target DNA, including cytosine 5-hydroxymethylation and, at least at some duplex positions, glucosyl-5-hydroxymethylation (Vlot et al., 2018). In this respect, Cas9 differs from other molecular systems, notably the ribosome and replicative DNA polymerases, which enhance the specificity of base-pairing by direct readout of base-pair shape and steric rejection of mispairs (Kunkel and Bebenek, 2000; Rodnina and Wintermeyer, 2001; Timsit, 1999). Secondly, Cas9 is a multidomain protein that displays considerable conformational dynamics and is therefore able to accommodate local distortions in the guide–TS duplex geometry by compensatory rearrangements of the REC2, REC3 and HNH domains. Indeed, in most off-target structures reported in this study, almost all atomic contacts between Cas9 and the guide–TS heteroduplex are preserved. Thus, Cas9 only detects guide-target mismatches by indirect readout of the guide RNA–TS DNA heteroduplex width, except at the PAM-distal end of the heteroduplex where base mismatches result in duplex unpairing, as discussed below. Our observations are consistent with recent molecular dynamics simulation studies showing that internally positioned mismatches within the guide RNA–TS DNA heteroduplex are readily incorporated within the heteroduplex and have only minor effects on Cas9 interactions

bioRxiv preprint doi: https://doi.org/10.1101/2021.11.18.469088; this version posted November 18, 2021. The copyright holder for this preprint (which was not certified by peer review) is the author/funder. All rights reserved. No reuse allowed without permission.

(Mitchell et al., 2020). The lack of a steric base-pair enforcement mechanism and the resulting off-target promiscuity likely reflects the biological function of Cas9 in CRISPR immunity, where mismatch tolerance contributes to interference by enabling the targeting of closely related viruses and hindering immune evasion by mutations or covalent base modifications (Deveau et al., 2008; Semenova et al., 2011; van Houte et al., 2016; Yaung et al., 2014).

Structural rigidity of the guide RNA seed region and implications for off-target recognition

The seed sequence of the Cas9 guide RNA (nucleotides 11-20) is the primary determinant of target DNA binding, a consequence of its structural pre-ordering in an A-like conformation by extensive interactions with Cas9 (Anders et al., 2014; Jiang et al., 2015; Nishimasu et al., 2014; Zhu et al., 2019). Our data indicate that structural rigidity of the guide RNA seed sequence also affects off-target recognition, as base mispairs in the seed region of the guide–off-target heteroduplex can only be accommodated by conformational distortions of the TS DNA, which is subject to only a few steric constraints, notably at position 20 due to interactions with the phosphate lock loop (Anders et al., 2014). The rigidity of the guide RNA seed sequence increases the energetic penalty of base mispairing in the seed region of the heteroduplex, and thus contributes to mismatch sensitivity of Cas9 within the seed region. Although structural distortions of TS DNA facilitate biding of off-target substrates containing seed mismatches, they may nevertheless inhibit off-target cleavage by steric hindrance of the HNH domain, thereby further contributing to the general mismatch intolerance of the guide RNA seed sequence. The contrasting structural plasticities of the guide RNA and TS DNA strands are manifested in the differential activities of Cas9 against off-targets containing rU-dG and rG-dT mismatches within the seed region (Boyle et al., 2021; Doench et al., 2016; Hsu et al., 2013; Jones et al., 2020; Zhang et al., 2020). Whereas rG-dT mismatches can be readily accommodated by wobble base pairing, seed sequence rigidity is expected to hinder rU-dG

bioRxiv preprint doi: https://doi.org/10.1101/2021.11.18.469088; this version posted November 18, 2021. The copyright holder for this preprint (which was not certified by peer review) is the author/funder. All rights reserved. No reuse allowed without permission.

wobble base pairing. Combined with a lower energetic penalty associated with rG-dT mismatch binding (binding an off-target with an rG-dT mismatch requires unpairing a dT-dA base pair in the off-target DNA, while rU-dG off-target recognition requires dC-dG unpairing), these effects thus help Cas9 discriminate against rU-dG mismatches in the seed region.

Recognition of off-targets containing insertions and deletions

Bona fide off-target sites containing insertions or deletions have been detected in a number of studies (Boyle et al., 2021; Cameron et al., 2017; Doench et al., 2016; Jones et al., 2020; Tsai et al., 2015). Nucleotide "bulging" has been proposed as a mechanism to recognize such an off-target, which would otherwise result in a large number of consecutive base mismatches. However, as Cas9 encloses the guide RNA–TS DNA heteroduplex in a central channel and makes extensive interactions along the entire length of the guide RNA strand, the formation of RNA bulges is precluded due to steric clashes, pointing to a different mechanism.

Indeed, the structures of *PTPRC-tgt2* off-target #1 and *FANCF* off-target #3 complexes reveal that off-target sequences predicted to contain single-nucleotide deletions in the seed region of the heteroduplex are instead recognized by base skipping, resulting in an unpaired guide RNA base within the duplex stack. Due to the lack of extensive contacts of Cas9 with the TS and the rigid coordination of the guide RNA in the seed region, these findings suggest that single nucleotide deletions can only be accommodated within the seed region of the heteroduplex and not elsewhere. This is supported by the observation that the *AAVS1* off-target #2 site, which was previously predicted to contain an RNA bulge or skip in the PAM-distal region (Cameron et al., 2017; Lazzarotto et al., 2020), is recognised via multiple mismatches.

Our structural observations indicate that *bona fide* off-targets predicted to contain single deletions within the seed region of the heteroduplex are recognized by base skipping, which incurs a large energetic penalty. As the seed region of the TS DNA is devoid of Cas9 contacts in the pre-cleavage state (Zhu et al., 2019), off-target sequences containing single-nucleotide

bioRxiv preprint doi: https://doi.org/10.1101/2021.11.18.469088; this version posted November 18, 2021. The copyright holder for this preprint (which was not certified by peer review) is the author/funder. All rights reserved. No reuse allowed without permission.

insertions in the seed region of the heteroduplex are likely to be recognized by DNA nucleotide bulging, likewise incurring a large energetic penalty as unwinding an off-target DNA sequence containing an insertion requires breaking an extra base pair. Additionally, TS DNA distortion might inhibit cleavage by steric hindrance of the HNH domain. These observations thus explain why Cas9 appears to tolerate mismatches better than insertions or deletions (Boyle et al., 2021; Cameron et al., 2017; Doench et al., 2016; Jones et al., 2020) and why deletions and insertions within the seed region are particularly deleterious. In contrast, off-target sequences containing insertions or deletions in the PAM-distal region of the heteroduplex, where both the guide RNA and TS DNA strands are contacted by Cas9, are instead likely to be bound in the unchanged register, with multiple base mispairs accommodated by non-canonical base pairing interactions. Our analysis suggests that a significant fraction of off-target sites previously predicted to contain insertions or deletions may be recognized in this manner.

PAM-distal base pairing and the conformational checkpoint of Cas9

Upon substrate DNA hybridization and R-loop formation, Cas9 undergoes conformational activation of its nuclease domains (Zhu et al., 2019). The Cas9 REC3 domain plays a key role in the process, as it senses the integrity of the PAM-distal region of the guide RNA–TS DNA heteroduplex and allosterically regulates the REC2 and HNH domains, providing a conformational checkpoint that traps Cas9 in a conformationally inactive state in the absence of PAM-distal hybridization (Chen et al., 2017; Dagdas et al., 2017; Palermo et al., 2018; Zhu et al., 2019). Our structural data confirm that mismatches at the PAM-distal end of the heteroduplex (positions 1-3) result in heteroduplex unpairing, incomplete R-loop formation and structural repositioning of the REC3 domain, indicating a perturbation of the Cas9 conformational checkpoint. We envision that the observed conformational state mimics the structural effect of 5’-truncated guide RNAs, which have been shown to improve targeting specificity (Fu et al., 2014). Furthermore, similarities with the structure of a high-fidelity Cas9

bioRxiv preprint doi: https://doi.org/10.1101/2021.11.18.469088; this version posted November 18, 2021. The copyright holder for this preprint (which was not certified by peer review) is the author/funder. All rights reserved. No reuse allowed without permission.

variant (Guo et al., 2019) suggest a shared underlying mechanism for increased specificity. In both cases, disruption of REC3 contacts with the PAM-distal heteroduplex modulates REC2/3 domain positioning, hindering allosteric activation of the HNH nuclease domain (Chen et al., 2017; Dagdas et al., 2017; Palermo et al., 2018). This is also consistent with observations that REC2/3 domain repositioning in Cas9 complexes with chimeric RNA-DNA guides modulates cleavage efficiency and results in increased specificity by slowing down conformational nuclease activation and promoting substrate DNA dissociation (Donohoue et al., 2021). In addition, the establishment of new HNH protein contacts with the heteroduplex, as observed in *FANCF* off-target #4, has been proposed to affect the active site positioning of the HNH domain (Mitchell et al., 2020; Ricci et al., 2019; Zeng et al., 2018). Indeed, it has been demonstrated that truncated guides result in reduced cleavage rates due to impaired HNH docking (Dagdas et al., 2017).

Implications for off-target prediction

Our structural data reveal that Cas9 plays a limited steric role in off-target discrimination insofar as only sensing the integrity and general shape of the guide–target heteroduplex. Off-target activity is thus largely determined by the kinetics and energetics of R-loop formation, *i.e.,* off-target DNA strand separation and guide RNA–TS DNA hybridization, and the Cas9 conformational activation checkpoint. We observe on multiple occasions in the determined off-target complexes that a given base mismatch adopts different conformational arrangements depending on its position along the guide RNA–TS DNA heteroduplex. This poses a challenge for *ab initio* modelling of off-target activity, as biophysical models of off-target binding and cleavage are bound to be of limited accuracy unless they incorporate position-dependent energetic penalties for each base mismatch type and for deletions, as well as position- and base-specific penalties for insertions (Boyle et al., 2021; Jones et al., 2020; Zhang et al., 2020). In addition, as certain off-target sequences that are incompatible with dsDNA cleavage can

bioRxiv preprint doi: https://doi.org/10.1101/2021.11.18.469088; this version posted November 18, 2021. The copyright holder for this preprint (which was not certified by peer review) is the author/funder. All rights reserved. No reuse allowed without permission.

undergo NTS nicking (Fu et al., 2019; Jones et al., 2020; Murugan et al., 2020; Zeng et al., 2018), future bioinformatic models need to be able to predict off-target nicking activity as well. Furthermore, accurate modelling of off-target interactions remains difficult due to context-dependent effects, as documented in previous studies showing that the binding and cleavage defects of consecutive mismatches deviate from additivity (Boyle et al., 2021; Cameron et al., 2017; Lazzarotto et al., 2020; Zhang et al., 2020). Indeed, our structural data rationalize this by showing that the conformation of a given base mismatch is highly sensitive to the presence of neighbouring mismatches. As seen in the case of *AAVS1* off-target #2 complex, multiple mismatched bases can synergistically combine to preserve an on-target-like heteroduplex conformation that passes the REC3 conformational checkpoint, supporting nearly on-target efficiencies of cleavage (Zhang et al., 2020). This is in line with recent cryo-EM structural studies suggesting that indirect readout of heteroduplex conformation is coupled to nuclease activation, while the presence of mismatches disrupts this coupling (Bravo et al., 2021; Pacesa and Jinek, 2021). Critically, reversion of one of the mismatches in this off-target substrate impairs cleavage activity. Similar effects have been described for other DNA binding proteins such as transcription factors, where mismatches modulate the binding activity of the protein by affecting the conformation of the DNA duplex (Afek et al., 2020). In an analogy with Cas9, these proteins check for correct binding sites through indirect sequence readout by sampling for the correct duplex shape rather than base sequence (Abe et al., 2015; Kitayner et al., 2010; Rohs et al., 2009a; Rohs et al., 2009b).

In conclusion, structural insights presented in this study establish an initial framework for understanding the molecular basis for the off-target activity of Cas9. In conjunction with ongoing computational studies, these findings will help achieve improved energetic parametrization of off-target mismatches and deletions/insertions, thus contributing to the development of more accurate off-target prediction algorithms and more specific guide RNA

bioRxiv preprint doi: https://doi.org/10.1101/2021.11.18.469088; this version posted November 18, 2021. The copyright holder for this preprint (which was not certified by peer review) is the author/funder. All rights reserved. No reuse allowed without permission.

designs. In doing so, these studies will contribute towards increasing the precision of CRISPR-Cas9 genome editing and the safety of its therapeutic applications.

bioRxiv preprint doi: https://doi.org/10.1101/2021.11.18.469088; this version posted November 18, 2021. The copyright holder for this preprint (which was not certified by peer review) is the author/funder. All rights reserved. No reuse allowed without permission.

Author contributions

M.P., P.C., P.D.D., and M.J. conceived the study. M.P. purified wild-type Cas9, performed *in vitro* cleavage assays, crystallized ternary Cas9 complexes, solved the structures, and performed structural analysis along with M.J.; A.C. performed switchSENSE binding measurements, under the supervision of F.H.T.A; M.J.I. performed the SITE-Seq assay; C-H.L. wrote the computational off-target classification model and P.D.D. and P.C. analysed the output; K.B. purified dCas9, transcribed sgRNAs, and prepared DNA substrates for in vitro cleavage assays; M.P., F.H.T.A., P.C., P.D.D., and M.J. wrote the manuscript.

Conflict of interest statement

P.D.D. and M.J.I are current employees of Caribou Biosciences, Inc., and C-H.L. and P.C. are former employees of Caribou Biosciences, Inc. M.J. is a co-founder of Caribou Biosciences, Inc. M.J., C-H.L., M.J.I., P.C. and P.D.D. are named inventors on patents and patent applications related to CRISPR-Cas technologies.

Acknowledgements

We thank members of the Jinek laboratory and Caribou Biosciences, Inc. for discussion and critical reading of the manuscript. We thank Vincent Olieric, Meitian Wang, and Takashi Tomizaki (Swiss Light Source, Paul Scherrer Institute) for assistance with crystallographic data collection and Nena Matscheko from Dynamic Biosensors for support with switchSENSE experiments. We thank the NCCR RNA and Disease for providing infrastructural support. This work was supported by the Swiss National Science Foundation Grant 31003A_182567 (to M.J.). M.J. is an International Research Scholar of the Howard Hughes Medical Institute and Vallee Scholar of the Bert L & N Kuggie Vallee Foundation.

bioRxiv preprint doi: https://doi.org/10.1101/2021.11.18.469088; this version posted November 18, 2021. The copyright holder for this preprint (which was not certified by peer review) is the author/funder. All rights reserved. No reuse allowed without permission.

Figures and Legends

Figure 1

a

Gene	Sequence	0	1	2	3	4	5	6	7	8	9	10	11	12	13	14	15	16	17	18	19	20	P	A	M
AAVS1	guide RNA	*G*	G	G	G	G	C	C	A	C	U	A	G	G	G	A	C	A	G	G	A	U			
AAVS1	on-target		C	C	C	C	G	G	T	G	A	T	C	C	C	T	G	T	C	C	T	A	A	C	C
AAVS1	off-target1		·	·	·	T	·	·	·	A	G	·	·	·	·	·	·	·	·	·	·	·	C	C	C
AAVS1	off-target2		A	·	·	·	C	·	G	T	G	·	·	·	·	·	·	·	·	·	A	·	A	C	C
AAVS1	off-target3		·	·	·	·	·	·	·	C	·	·	·	·	·	·	C	·	·	·	·	·	T	C	C
AAVS1	off-target4		A	·	·	·	·	·	·	·	·	·	A	·	·	·	·	·	·	·	·	T	A	C	C
AAVS1	off-target5		·	·	·	T	·	·	·	·	·	C	·	·	·	·	·	·	·	·	G	G	A	C	C
FANCF	guide RNA	*G*	G	G	A	A	U	C	C	C	U	U	C	U	G	C	A	G	C	A	C	C			
FANCF	on-target		C	C	T	T	A	G	G	G	A	A	G	A	C	G	T	C	G	T	G	G	A	C	C
FANCF	off-target1		·	·	·	·	G	·	·	·	C	·	·	·	·	·	·	·	·	·	·	·	T	C	C
FANCF	off-target2		·	·	·	C	·	·	·	·	·	G	·	·	T	·	·	·	·	·	·	·	T	C	C
FANCF	off-target3	*G*	·	·	·	C	G	·	·	·	·	·	·	·	·	·	·	·	—	·	·	·	G	C	C
FANCF	off-target4		T	G	G	·	·	·	·	·	·	G	·	·	·	·	·	·	·	·	·	·	A	C	C
FANCF	off-target5		A	·	·	·	·	·	·	·	T	·	·	·	G	·	·	·	·	·	·	·	A	C	C
FANCF	off-target6		·	·	·	·	G	T	·	·	·	·	·	·	·	·	·	·	·	A	·	·	T	C	C
FANCF	off-target7		·	·	·	·	·	·	T	·	·	·	A	·	T	·	·	·	·	·	·	·	T	C	C
PTPRC	guide RNA	*G*	G	C	A	A	A	A	C	U	C	A	A	C	C	C	U	A	C	C	C	C			
PTPRC	on-target		C	G	T	T	T	T	G	A	G	T	T	G	G	G	A	T	G	G	G	G	A	C	C
PTPRC	off-target1	*T*	·	·	·	·	A	·	·	T	·	·	·	·	·	·	—	·	·	·	·	·	A	C	C
TRAC	guide RNA	*G*	A	G	A	G	U	C	U	C	U	C	A	G	C	U	G	G	U	A	C	A			
TRAC	on-target		T	C	T	C	A	G	A	G	A	G	T	C	G	A	C	C	A	T	G	T	G	C	C
TRAC	off-target1		C	T	·	·	·	·	·	·	G	·	·	·	·	·	T	·	·	·	·	·	A	C	C
TRAC	off-target2		·	T	·	·	·	·	T	·	T	·	·	·	·	·	·	·	·	·	·	·	A	C	C

b

Gene	Target	(%) 24h cleavage	k_{obs} (s^{-1})	k_{on} ($M^{-1} . s^{-1}$)	k_{off} (s^{-1})	K_d (pM)	24h cleavage PAMmer (%)	k_{obs} (s^{-1}) PAMmer
AAVS1	on-target	92.2	1.6240	3.95E+06	5.74E-05	14.5	95.0	0.5622
AAVS1	off-target1	92.7	0.0713	4.73E+06	6.29E-05	13.3	87.5	0.2390
AAVS1	off-target2	95.1	0.0337	8.76E+06	3.38E-03	386.0	85.5	0.0040
AAVS1	off-target3	96.7	0.0511	3.30E+06	2.51E-03	761.0	82.7	0.0806
AAVS1	off-target4	94.4	0.0039	1.09E+07	3.28E-03	301.0	89.6	0.0645
AAVS1	off-target5	18.9	0.0001	ND	ND	ND	70.1	0.0068
FANCF	on-target	97.5	0.2383	3.45E+06	7.46E-05	21.6	98.3	0.5654
FANCF	off-target1	35.1	0.0006	3.97E+06	2.09E-03	528.0	97.4	0.0693
FANCF	off-target2	62.4	0.0006	1.42E+06	2.45E-03	1730.0	92.9	0.2333
FANCF	off-target3	0.0	0.0000	1.22E+07	2.37E-03	193.0	4.2	0.0000
FANCF	off-target4	53.0	0.0005	3.35E+06	1.91E-03	571.0	38.9	0.0011
FANCF	off-target5	80.4	0.0010	1.27E+06	2.55E-03	2010.0	92.9	0.0584
FANCF	off-target6	8.2	0.0001	1.50E+06	2.03E-03	1350.0	66.6	0.0007
FANCF	off-target7	5.2	0.0036	2.95E+06	3.21E-03	1090.0	94.5	0.0134
PTPRC	on-target	96.8	0.4588	6.08E+06	2.19E-04	36.0	95.5	0.0741
PTPRC	off-target1	0.0	0.0000	1.22E+07	2.39E-03	196.0	91.4	0.0012
TRAC	on-target	97.7	0.3808	1.02E+07	3.23E-04	31.8	93.5	0.1812
TRAC	off-target1	95.8	0.0195	1.37E+06	1.77E-04	130.0	90.7	0.0807
TRAC	off-target2	65.0	0.0007	9.43E+06	3.27E-04	34.6	88.4	0.0260

c

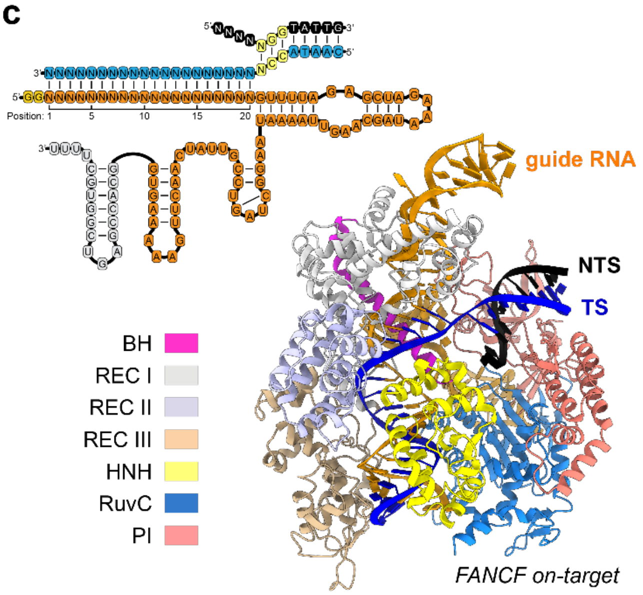

bioRxiv preprint doi: https://doi.org/10.1101/2021.11.18.469088; this version posted November 18, 2021. The copyright holder for this preprint (which was not certified by peer review) is the author/funder. All rights reserved. No reuse allowed without permission.

Figure 1. Biochemical and structural analysis of Cas9 off-targets.

(**A**) Guide RNA and (off-)target DNA sequences selected for biochemical and structural analysis. Matching bases in off-targets are denoted by a dot; nucleotide mismatches and deletions (–) are highlighted. (**B**) Kinetic and thermodynamic parameters of off-target substrates. The cleavage rate constants (k_{obs}) were derived from single-exponential function fitting of measured cleavage rates. The binding and dissociation rate constants (k_{on} and k_{off}) and the equilibrium dissociation constant (K_d) were determined using a DNA nanolever binding (switchSENSE) assay. (**C**) Top: Schematic representation of the guide RNA (orange), TS (blue), and NTS (black) sequences used for crystallisation. The PAM sequence in the DNA is highlighted in yellow. Bottom: Structure of the Cas9 *FANCF* on-target complex. Individual Cas9 domains are coloured according to the legend; substrate DNA target strand (TS) is coloured blue, non-target strand (NTS) black, and the guide RNA orange.

bioRxiv preprint doi: https://doi.org/10.1101/2021.11.18.469088; this version posted November 18, 2021. The copyright holder for this preprint (which was not certified by peer review) is the author/funder. All rights reserved. No reuse allowed without permission.

Figure 2

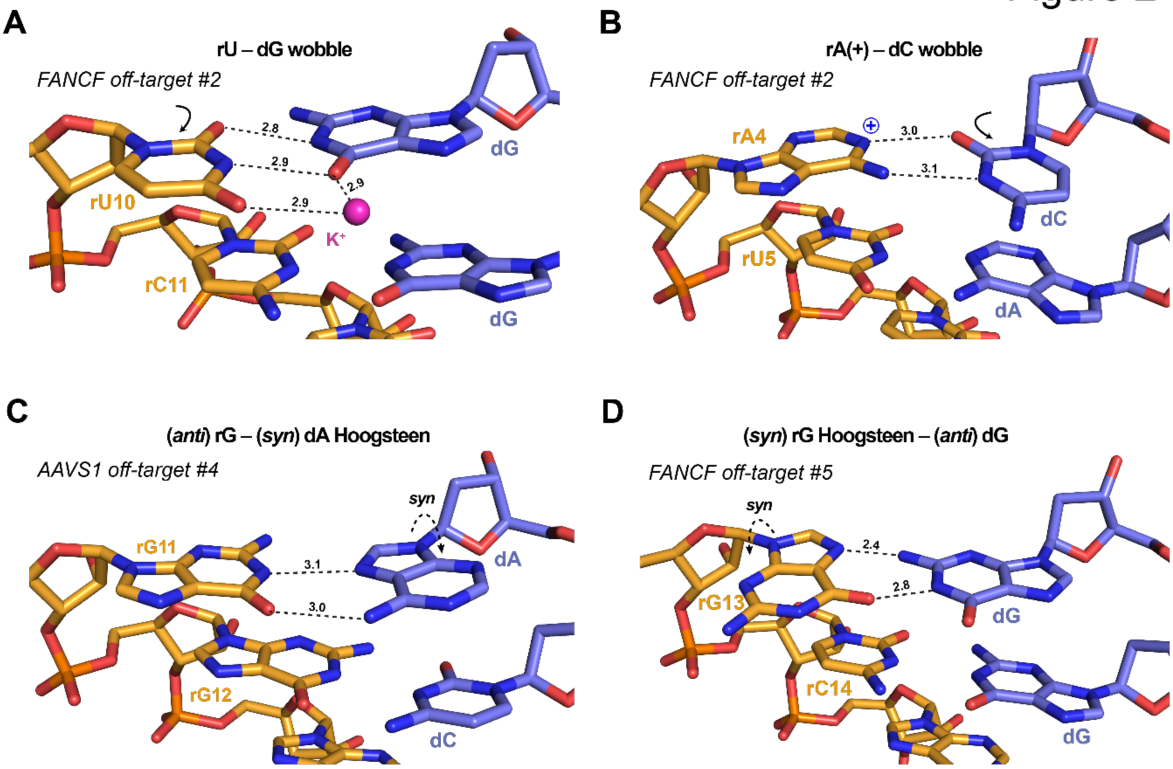

Figure 2. Cas9 off-target binding is enabled by non-canonical base pairing.

Close-up views of (**A**) rU-dG wobble base pair at duplex position 10 in *FANCF* off-target #2 complex, (**B**) rA-dC wobble base pair at position 4 in *FANCF* off-target #2 complex, (**C**) rG-dA Hoogsteen base pair at duplex position 11 in *AAVS1* off-target #4 complex and (**D**) rG-dG Hoogsteen base pair at duplex position 13 in *FANCF* off-target #5 complex. Hydrogen bonding interactions are indicated with dashed lines. Numbers indicate interatomic distances in Å. Solid arrows indicate conformational changes relative to the corresponding on-target complex structures. Dashed arrows indicate *anti-syn* isomerization of the dA and rG bases to enable Hoogsteen-edge base pairing. A bound monovalent ion, modelled as K^+, is depicted as a purple sphere.

bioRxiv preprint doi: https://doi.org/10.1101/2021.11.18.469088; this version posted November 18, 2021. The copyright holder for this preprint (which was not certified by peer review) is the author/funder. All rights reserved. No reuse allowed without permission.

Figure 3

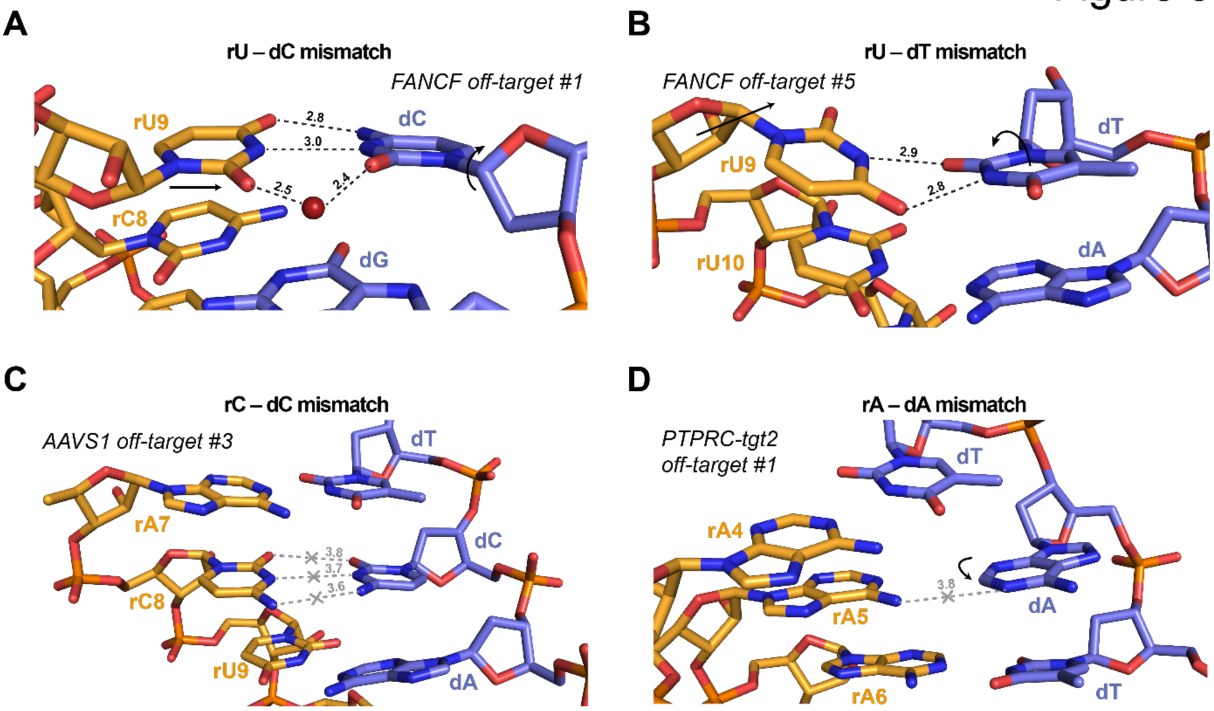

Figure 3. Duplex backbone distortions facilitate formation of non-canonical base pairs. (**A**) Close-up view of the rU-dC base pair at duplex position 9 in *FANCF* off-target #1 complex, facilitated by lateral displacement of the guide RNA backbone (solid arrow). Hydrogen bonding interactions are indicated with dashed lines. Solid arrows indicate conformational changes relative to the on-target complex. Numbers indicate interatomic distances in Å. Bound water molecule is depicted as red sphere. (**B**) Zoomed-in view of the rU-dT base pair at position 9 in *FANCF* off-target #5 complex. Solid arrows indicate lateral displacement of the rU nucleotide and propeller twist of the dT base. (**C**) Zoomed-in view of the rC-dC mispair at duplex position 8 in *AAVS1* off-target #3 complex. The distances between the cytosine bases indicate lack of hydrogen bonding. (**D**) Zoomed-in view of the rA-dA mispair at duplex position 5 in *PTPRC-tgt2* off-target #1 complex.

bioRxiv preprint doi: https://doi.org/10.1101/2021.11.18.469088; this version posted November 18, 2021. The copyright holder for this preprint (which was not certified by peer review) is the author/funder. All rights reserved. No reuse allowed without permission.

Figure 4

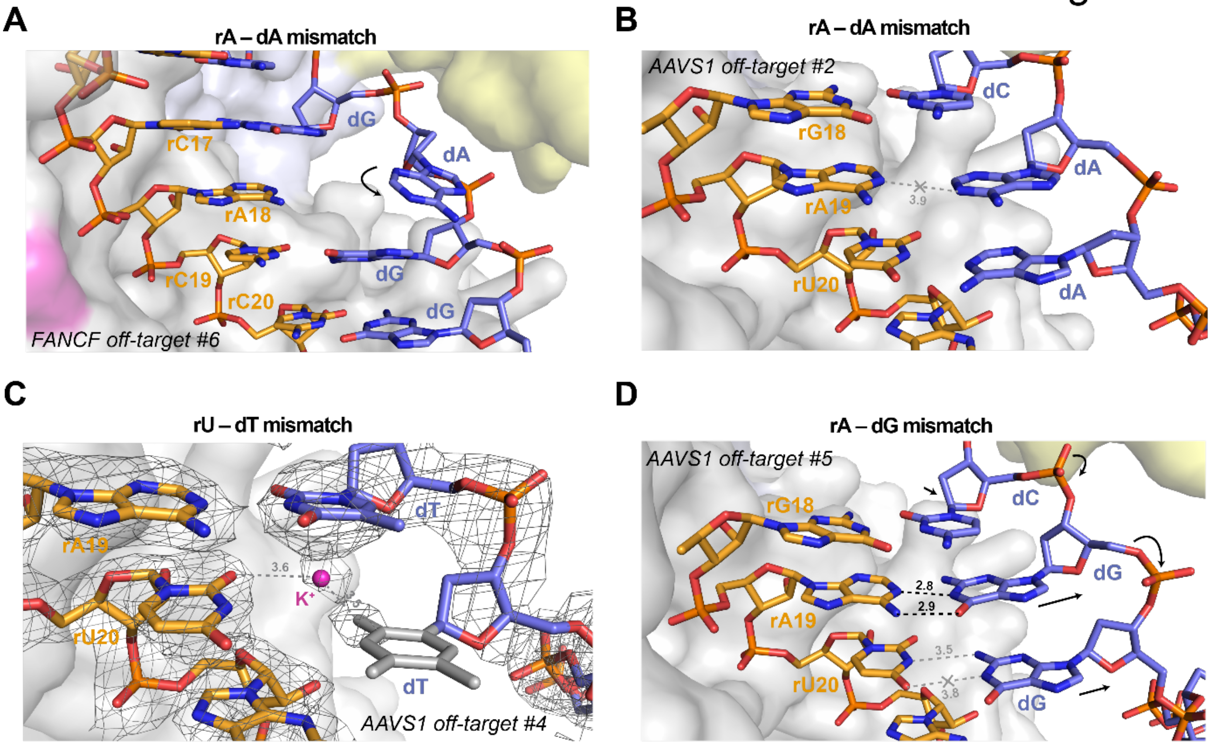

Figure 4. **TS distortion facilitates mismatch accommodation in the seed region of the guide–off-target heteroduplex.**

(**A**) Close-up view of the rA-dA mismatch at position 18 in *FANCF* off-target #6 complex, showing major groove extrusion of the dA base. (**B**) Close-up view of the rA-dA mismatch at position 19 in *AAVS1* off-target #2 complex, showing retention of the dA base in the duplex stack. (**C**) Close-up rU-dT mispair at the PAM-proximal position 20 in *AAVS1* off-target #4 complex. Residual electron density indicates the presence of an ion or solvent molecule. Refined 2mF_o−DF_c electron density map of the heteroduplex, contoured at 1.5σ, is rendered as a grey mesh. Structurally disordered thymine nucleobase for which no unambiguous density is present is in grey. (**D**) Zoomed-in view of the rA-dG base pair at position 19 and the unpaired rU-dG mismatch at position 20 in *AAVS1* off-target #5 complex. Arrows indicate conformational changes in the TS backbone relative to the on-target complex.

bioRxiv preprint doi: https://doi.org/10.1101/2021.11.18.469088; this version posted November 18, 2021. The copyright holder for this preprint (which was not certified by peer review) is the author/funder. All rights reserved. No reuse allowed without permission.

Figure 5

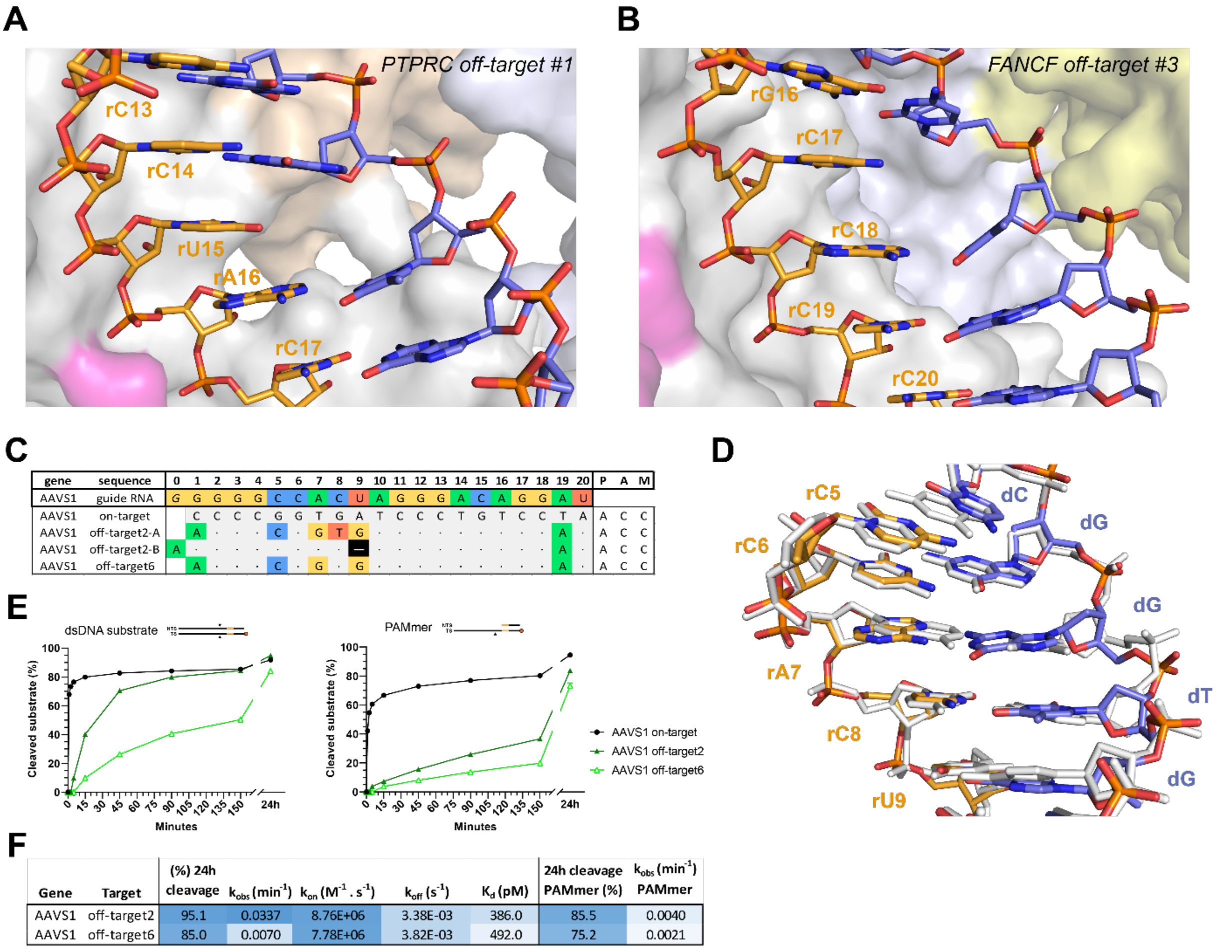

gene	sequence	0	1	2	3	4	5	6	7	8	9	10	11	12	13	14	15	16	17	18	19	20	P	A	M
AAVS1	guide RNA	*G*	G	G	G	G	C	C	A	C	U	A	G	G	G	A	C	A	G	G	A	U			
AAVS1	on-target		C	C	C	C	G	G	T	G	A	T	C	C	C	T	G	T	C	C	T	A	A	C	C
AAVS1	off-target2-A		A	·	·	·	C	·	G	T	G	·	·	·	·	·	·	·	·	·	A	·	A	C	C
AAVS1	off-target2-B	A	·	·	·	·	·	·	·	·	—	·	·	·	·	·	·	·	·	·	A	·	A	C	C
AAVS1	off-target6		A	·	·	·	C	·	G	·	G	·	·	·	·	·	·	·	·	·	A	·	A	C	C

Gene	Target	(%) 24h cleavage	k_{obs} (min^{-1})	k_{on} (M^{-1} . s^{-1})	k_{off} (s^{-1})	K_d (pM)	24h cleavage PAMmer (%)	k_{obs} (min^{-1}) PAMmer
AAVS1	off-target2	95.1	0.0337	8.76E+06	3.38E-03	386.0	85.5	0.0040
AAVS1	off-target6	85.0	0.0070	7.78E+06	3.82E-03	492.0	75.2	0.0021

Figure 5. Off-targets with single-nucleotide deletions are accommodated by base skipping or multiple consecutive mismatches.

(**A**) Zoomed-in view of the base skip at duplex position 15 in the *PTPRC-tgt2* off-target #1 complex. (**B**) Zoomed-in view of the base skip at duplex position 17 in the *FANCF* off-target #3 complex. (**C**) Schematic depiction of alternative base pairing interactions in the *AAVS1* off-target #2 complex. *AAVS1* off-target #6 substrate was designed based on the *AAVS1* off-target #2, with the reversal of a single mismatch in the consecutive region back to the corresponding canonical base pair. (**D**) Structural overlay of the *AAVS1* off-target #2 (coloured) and *AAVS1* on-target (white) heteroduplexes. (**E**) Cleavage DNA kinetics of AAVS1 on-target, off-target #2 and off-target #6 substrates. (**F**) Kinetic and thermodynamic parameters determined for *AAVS1* off-target #2 and #6 substrates. The apparent cleavage rate constants (k_{obs}) were derived

bioRxiv preprint doi: https://doi.org/10.1101/2021.11.18.469088; this version posted November 18, 2021. The copyright holder for this preprint (which was not certified by peer review) is the author/funder. All rights reserved. No reuse allowed without permission.

from a single-exponential function fitting of measured cleavage. Substrate binding (k_{on}) and dissociation (k_{off}) constants were determined using SwitchSENSE assay.

bioRxiv preprint doi: https://doi.org/10.1101/2021.11.18.469088; this version posted November 18, 2021. The copyright holder for this preprint (which was not certified by peer review) is the author/funder. All rights reserved. No reuse allowed without permission.

Figure 6

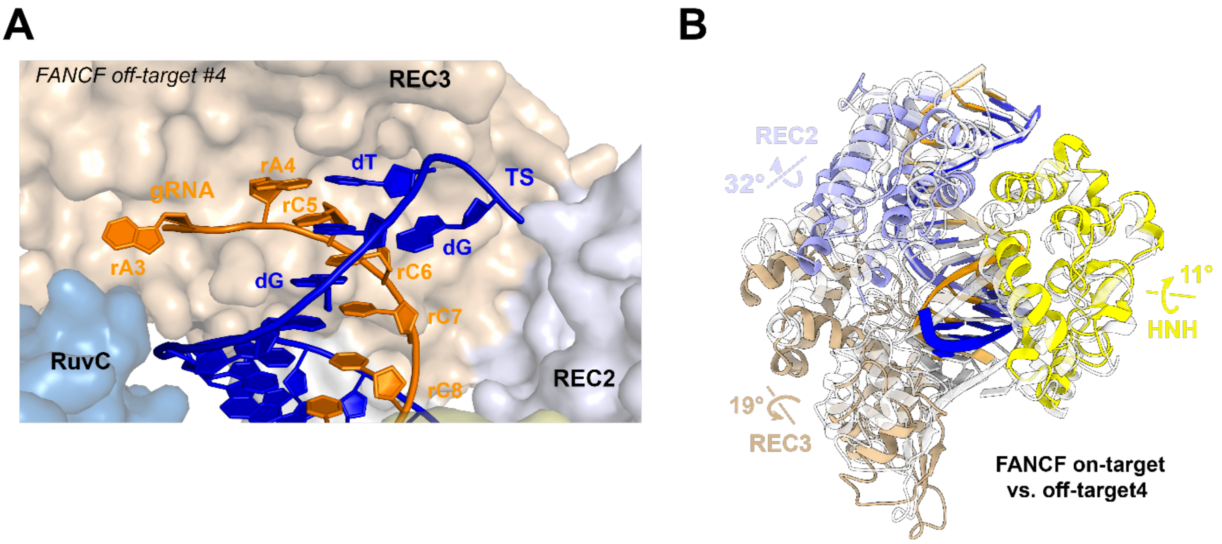

Figure 6. *FANCF* off-target #4 exhibits conformational changes in the REC2/3 and HNH domains due to PAM-distal duplex unpairing.

(**A**) Close-up view of the unpairing of mismatched bases at the PAM-distal end of the *FANCF* off-target #4 heteroduplex. The last two nucleotides on each strand could not be modelled due to structural disorder. (**B**) Overlay of the *FANCF* off-target #4 and *FANCF* on-target complex structures. The *FANCF* off-target #4 complex is coloured according to the domain legend in **Figure 1A**, *FANCF* on-target complex is shown in white. The REC1, RuvC, and PAM-interaction domains have been omitted for clarity, as no structural differences are observed.

bioRxiv preprint doi: https://doi.org/10.1101/2021.11.18.469088; this version posted November 18, 2021. The copyright holder for this preprint (which was not certified by peer review) is the author/funder. All rights reserved. No reuse allowed without permission.

Figure S1

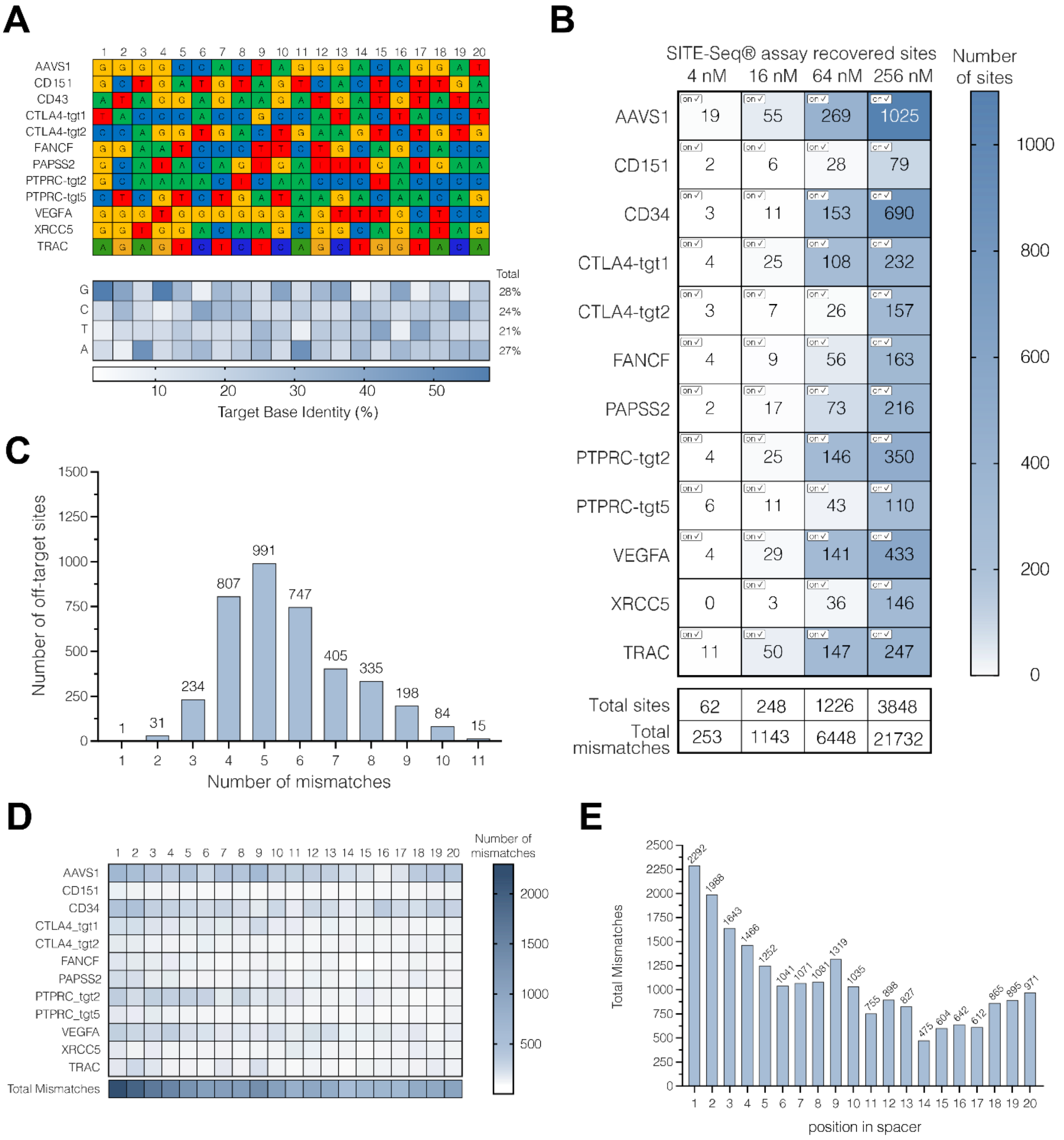

Figure S1. Off-target profiling of selected genomic sites using SITE-Seq.

(**A**) Selected genomic targets and the corresponding guide RNA sequences selected for the SITE-Seq assay off-target profiling. Heatmap indicates frequency of nucleotide identity across each position for the selected targets. (**B**) SITE-seq assay analysis for RNPs assembled with indicated crRNAs. The numbers of detected off-target sites are shown as a function of RNP concentration. Checked boxes indicate recovery of the on-target site. n=3 replicates per sample. (**C**) Number of off-target sites recovered by the SITE-Seq assay are shown as a function of the

bioRxiv preprint doi: https://doi.org/10.1101/2021.11.18.469088; this version posted November 18, 2021. The copyright holder for this preprint (which was not certified by peer review) is the author/funder. All rights reserved. No reuse allowed without permission.

number of mismatches between the guide RNA and the off-target sequence. (**D**) Frequency of nucleotide mismatches at each guide RNA–off-target DNA heteroduplex position for all off-target sites identified in (B). (**E**) Number of total identified mismatches per heteroduplex position.

bioRxiv preprint doi: https://doi.org/10.1101/2021.11.18.469088; this version posted November 18, 2021. The copyright holder for this preprint (which was not certified by peer review) is the author/funder. All rights reserved. No reuse allowed without permission.

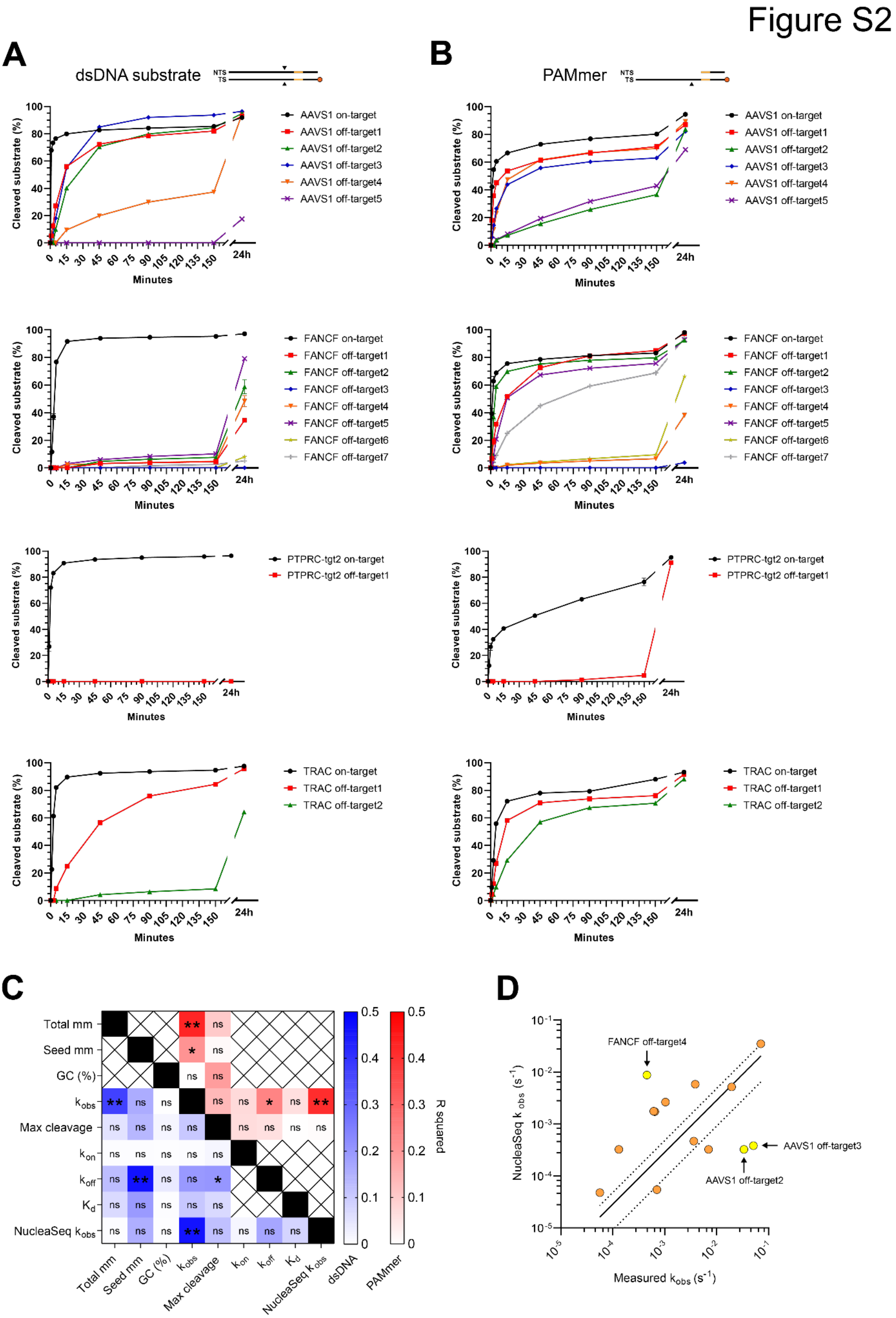

746

747 **Figure S2. *in vitro* cleavage of selected Cas9 off-target substrates.**

bioRxiv preprint doi: https://doi.org/10.1101/2021.11.18.469088; this version posted November 18, 2021. The copyright holder for this preprint (which was not certified by peer review) is the author/funder. All rights reserved. No reuse allowed without permission.

(**A**) *In vitro* clevage kinetics of fully double stranded on- and off-target DNA substrates for each guide RNA used in the study. Black triangles in the substrate schematic (top) indicate position of cleavage sites. Each data point represents a mean of four independent replicates. Error bars represent standard deviation for each time point. (**B**) *In vitro* clevage kinetics of partially single stranded (PAMmer) on- and off-target substrates. (**C**) Heatmap representation of mutual correlations between measured kinetic and thermodymamic parameters including cleavage (k_{obs}), substrate DNA binding (k_{on}), substrate dissociation (k_{off}) rate constants, equilibrium dissociation constant (K_d) with numbers of nucleotide mismatches in the off- target sites (total and within seed), the GC content of the spacer (%GC) and cleavage rate predicted using the NucleaSeq algorithm (NucleaSeq k_{obs}). The values were calculated across all off-targets for both dsDNA (lower left half, in blue), and partially single stranded (PAMmer) substrates (upper right half, in red). ns, no significant correlation. (**D**) Correlation between measured and NucleaSeq-predicted k_{obs} rate constants. Off-target sites with significant deviations are highlighted in yellow.

bioRxiv preprint doi: https://doi.org/10.1101/2021.11.18.469088; this version posted November 18, 2021. The copyright holder for this preprint (which was not certified by peer review) is the author/funder. All rights reserved. No reuse allowed without permission.

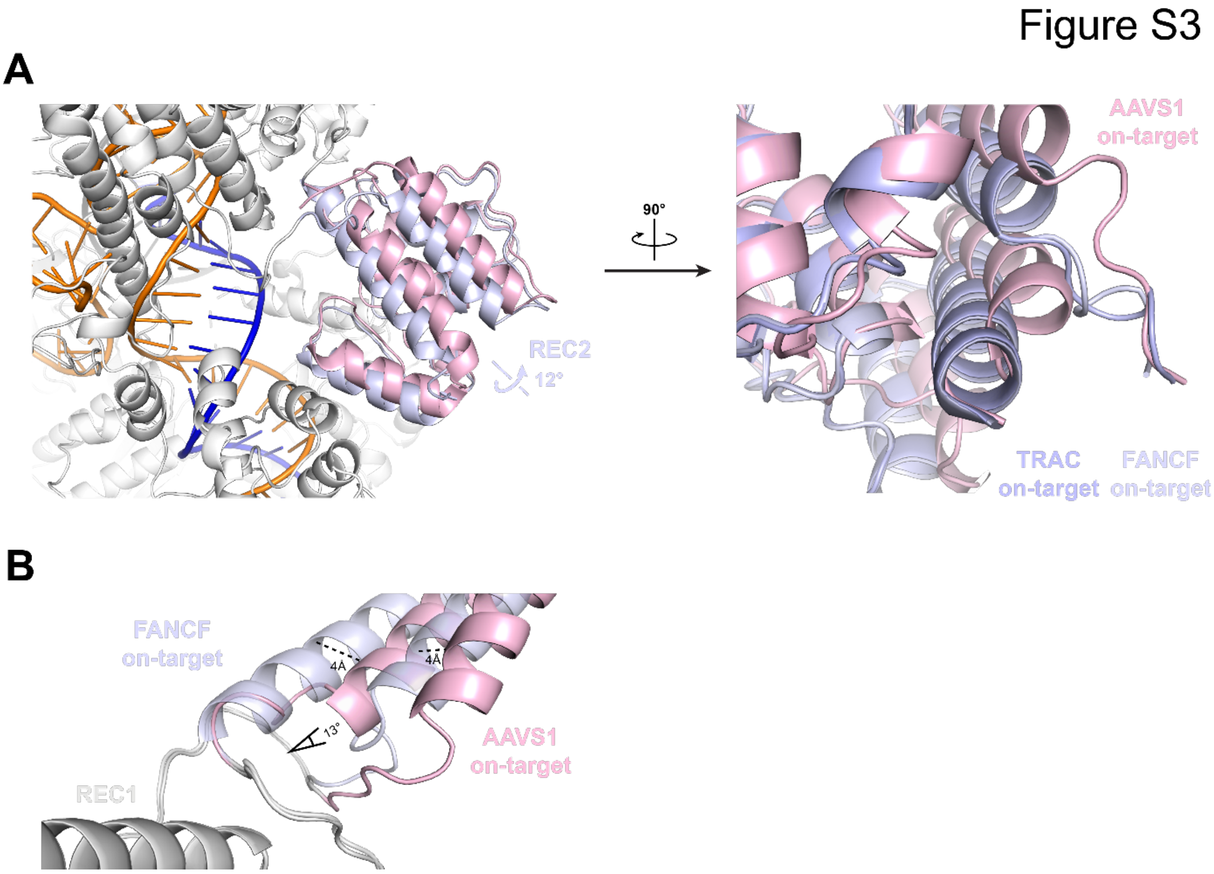

Figure S3. Alternative REC2 conformation in AAVS1 on-target.

(**A**) Overlay of REC2 domain conformations in the *AAVS1* (pink), *FANCF* (purple) and *TRAC* (light blue) on-target complexes (**B**) Close-up view of helix REC2 helix spanning Cas9 residues 174-180. Linear and angular displacements of the helix in the *AAVS1* on-target complex relative to the *FANCF* and *TRAC* on-target complexes are indicated.

bioRxiv preprint doi: https://doi.org/10.1101/2021.11.18.469088; this version posted November 18, 2021. The copyright holder for this preprint (which was not certified by peer review) is the author/funder. All rights reserved. No reuse allowed without permission.

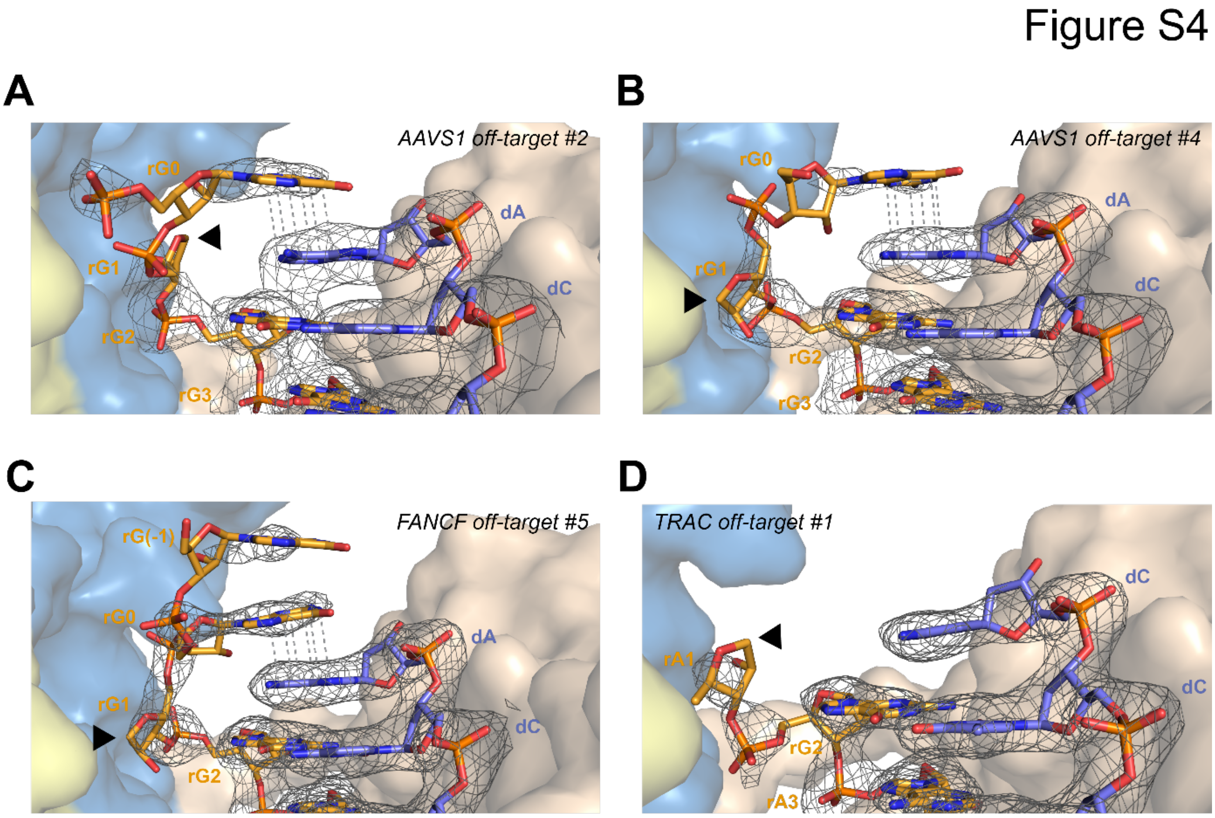

Figure S4. PAM-distal mismatches result in unpairing and disordering of guide RNA nucleobase in position 1.

Close-up views of the PAM-distal end of the guide RNA-TS heteroduplex in (**A**) *AAVS1* off-target #2, (**B**) *AAVS1* off-target #4, (**C**) *FANCF* off-target #5 and (**D**) *TRAC* off-target #1 complexes. Arrowheads indicate nucleotides with disordered bases. Refined 2mF_o–DF_c electron density maps of the heteroduplexes are rendered as a grey mesh and contoured at 1.2σ for (A) and 1.0σ for (B)-(D).

bioRxiv preprint doi: https://doi.org/10.1101/2021.11.18.469088; this version posted November 18, 2021. The copyright holder for this preprint (which was not certified by peer review) is the author/funder. All rights reserved. No reuse allowed without permission.

Figure S5

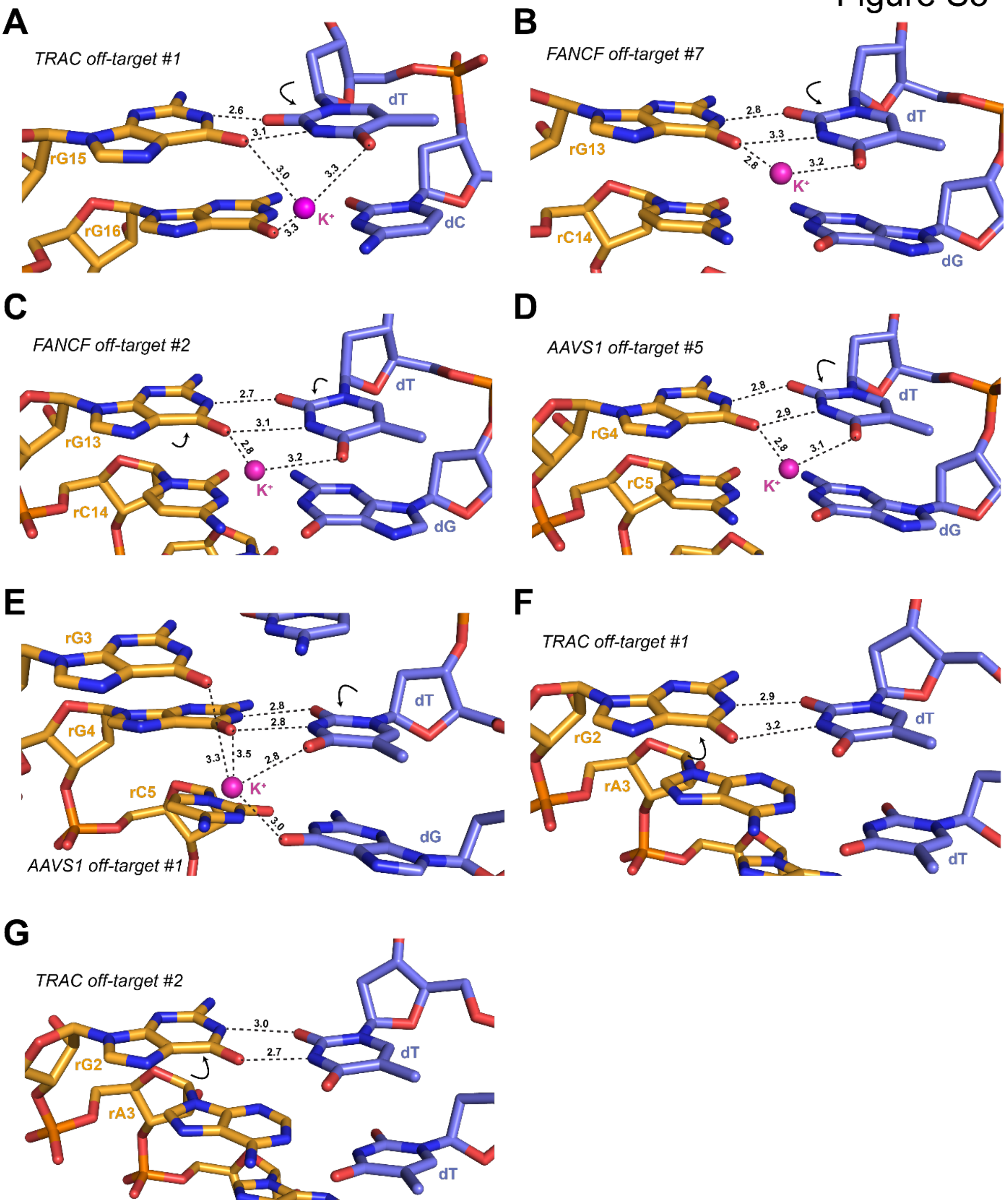

Figure S5. Wobble base pairing of rG-dT mismatches.

Close-up views of rG-dT mismatches at (**A**) heteroduplex position 15 in the *TRAC* off-target #1 complex, (**B**) position 13 in *FANCF* off-target #7 complex, (**C**) position 13 in *FANCF* off-target #2 complex, (**D**) position 4 in *AAVS1* off-target #5 complex, (**E**) position 4 in *AAVS1* off-target #1 complex, (**F**) position 2 in *TRAC* off-target #1 complex and (**G**) position 2 in *TRAC*

bioRxiv preprint doi: https://doi.org/10.1101/2021.11.18.469088; this version posted November 18, 2021. The copyright holder for this preprint (which was not certified by peer review) is the author/funder. All rights reserved. No reuse allowed without permission.

off-target #2 complex. Arrows indicate conformational changes relative to the corresponding on-target complex structures. Monovalent ions, modeled as K^+, are depicted as purple spheres. In (A)-(E), the dT base is displaced into the major groove and forms a canonical wobble base pair with the rG base. In (F)-(G), the the rG base instead shifts towards the minor groove to facilitate wobble pairing.

bioRxiv preprint doi: https://doi.org/10.1101/2021.11.18.469088; this version posted November 18, 2021. The copyright holder for this preprint (which was not certified by peer review) is the author/funder. All rights reserved. No reuse allowed without permission.

Figure S6

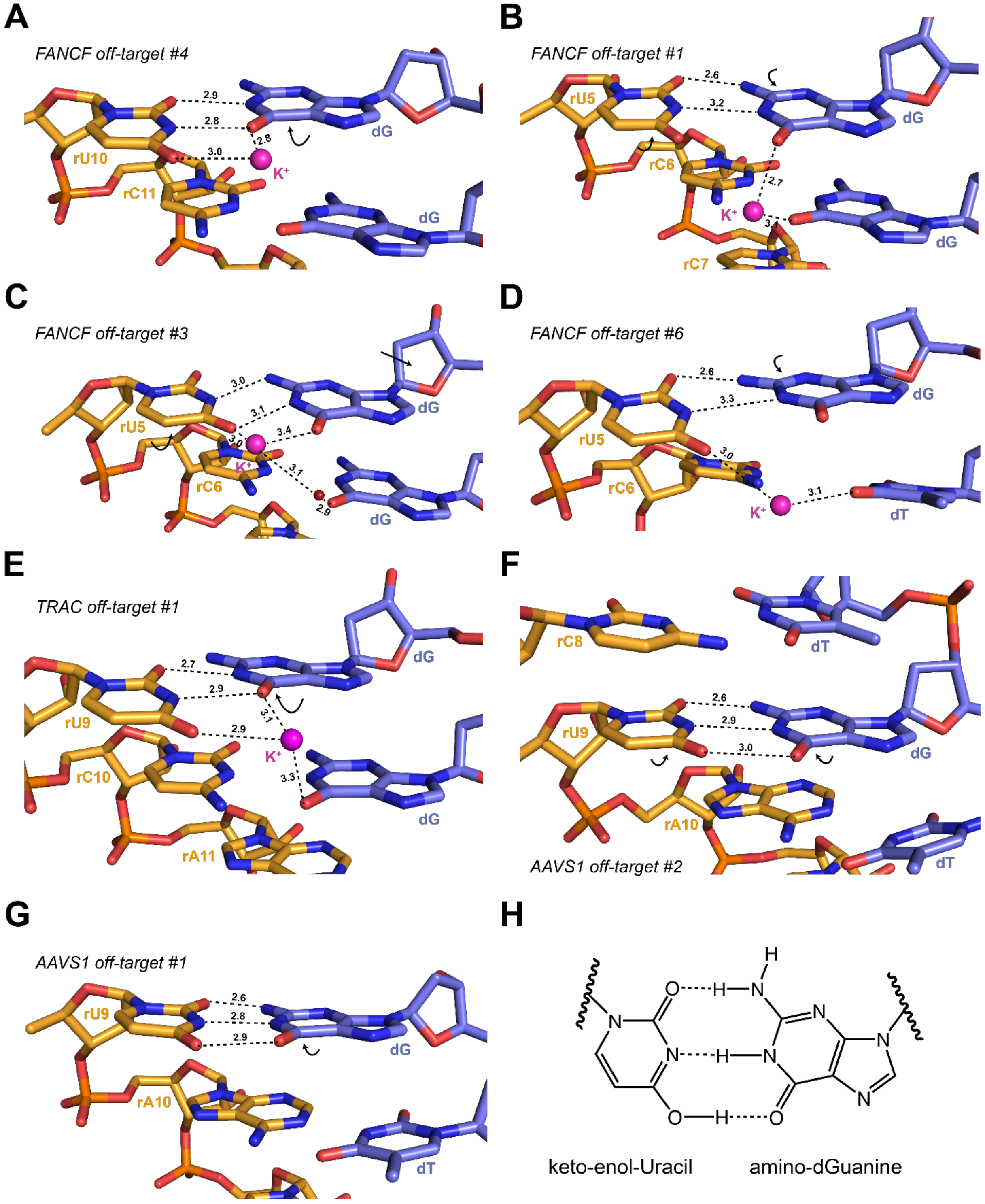

Figure S6. rU-dG wobble base pairs adopt duplex position-dependent conformations.

Close-up views of of rU-dG mispairs at (**A**) heteroduplex position 10 in *FANCF* off-target #4 complex, (**B**) position 5 in *FANCF* off-target #1 complex, (**C**) position 5 in *FANCF* off-target #3 complex, (**D**) position 5 in *FANCF* off-target #6 complex, (**E**) *TRAC* off-target #1 complex,

bioRxiv preprint doi: https://doi.org/10.1101/2021.11.18.469088; this version posted November 18, 2021. The copyright holder for this preprint (which was not certified by peer review) is the author/funder. All rights reserved. No reuse allowed without permission.

and (**F**) *AAVS1* off-target #2, and (**G**) *AAVS1* off-target #1 complex. Arrows indicate conformational changes relative to the corresponding on-target complex structures. Bound potassium ions are depicted as purple spheres. In (A), rU-dG wobble base pairing is achieved by minor groove displacement of the guanine base. In (B)-(D), the rU-dG mispairs adopt atypical conformations. In (E), the guanine base is shifted into the minor groove to form a wobble base pair, whereas at the identical heteroduplex position in (F) and (G), the rU-dG base pairs do not engage in wobble pairing, instead adopting alternative tautomeric forms. **(H)** Schematic depicting hydrogen bonding interactions between rU and dG bases in (F) and (G).

bioRxiv preprint doi: https://doi.org/10.1101/2021.11.18.469088; this version posted November 18, 2021. The copyright holder for this preprint (which was not certified by peer review) is the author/funder. All rights reserved. No reuse allowed without permission.

Figure S7

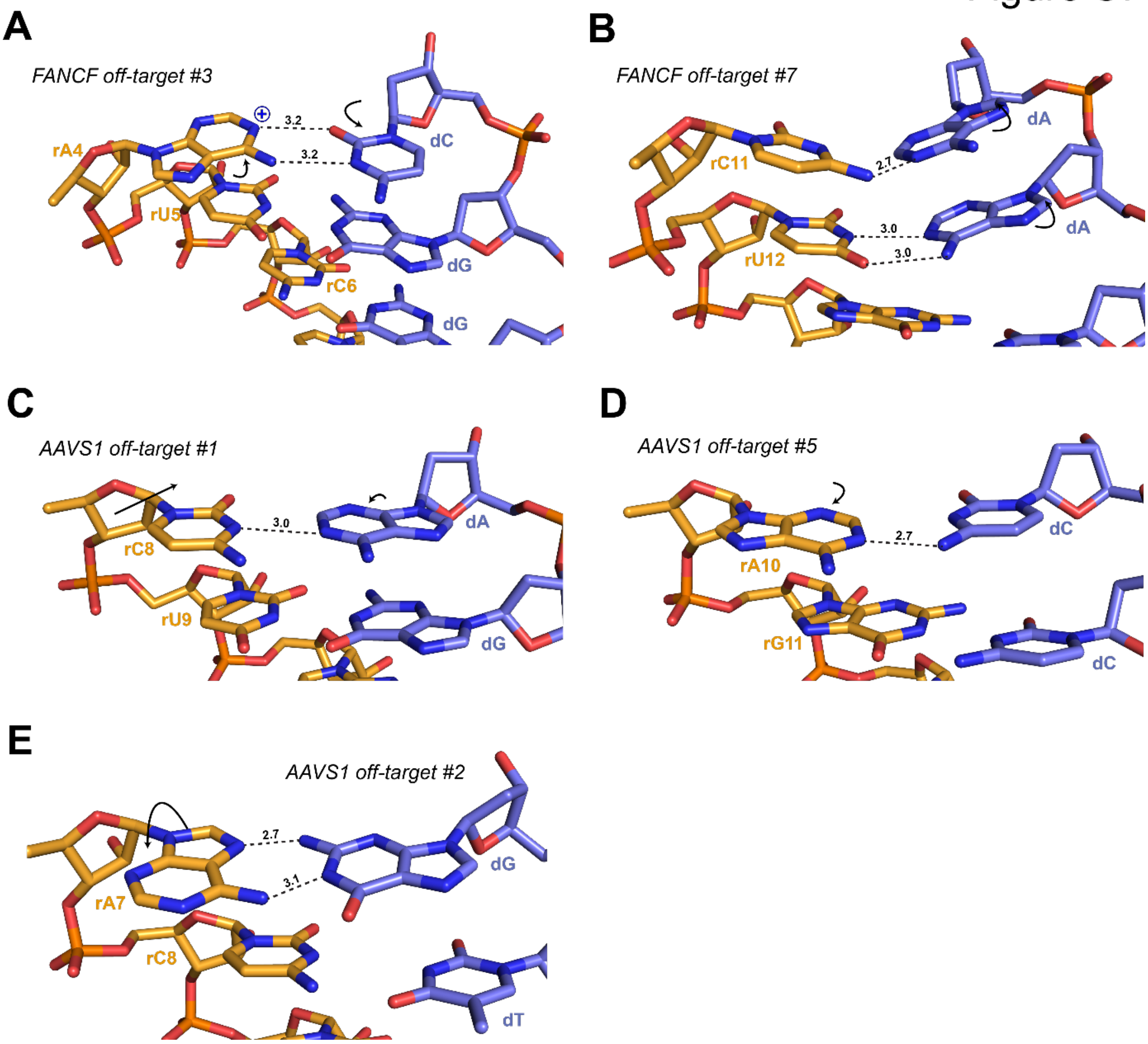

Figure S7. Additional non-canonical base pairs within Cas9 off-target complexes. (**A**) Close-up view of rA-dC wobble base pairing at position 4 in *FANCF* off-target #3 complex. The base pair geometry is consistent with base protonation or tautomerism to enable productive hydrogen bonding between the bases. (**B**) Close-up view of rC-dA mismatch at position 11 of *FANCF* off-target #7 complex, facilitated by base tilting at positions 11 and 12. (**C**) Close-up view of partially paired rC-dA mismatch at position 8 in *AAVS1* off-target #1 complex. (**D**) Close-up view of rA-dC mispair at position 10 in *AAVS1* off-target #5 complex. (**E**) Close-up view of Hoogsteen-edge rA-dG base pair at position 7 in *AAVS1* off-target #2 complex. Arrows indicate conformational changes relative to the corresponding on-target complexes.

bioRxiv preprint doi: https://doi.org/10.1101/2021.11.18.469088; this version posted November 18, 2021. The copyright holder for this preprint (which was not certified by peer review) is the author/funder. All rights reserved. No reuse allowed without permission.

Figure S8

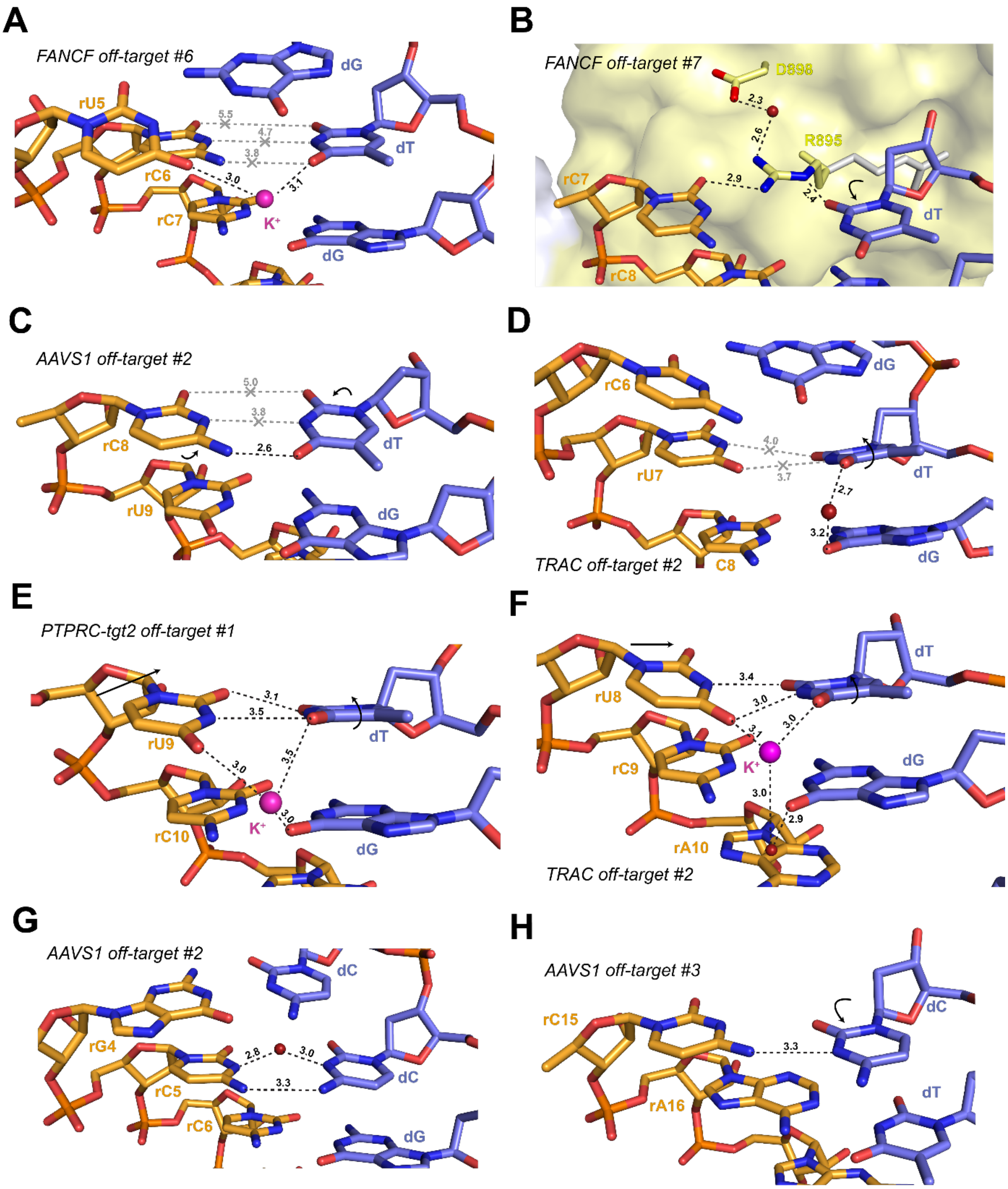

Figure S8. Preservation of base stacking in pyrimidine-pyrimidine off-target mismatches. (**A**) Close-up view of rC-dT mispair at position 6 in *FANCF* off-target #6 complex. (**B**) Close-up view of rC-dT mispair at position 7 in *FANCF* off-target #7 complex, bridged by Arg895. The arginine sidechain in the corresponding on-target complex is shown in white. (**C**) Close-up view of rC-dT base pairing at position 8 of *AAVS1* off-target #2. (**D**) Close-up view of rU-

bioRxiv preprint doi: https://doi.org/10.1101/2021.11.18.469088; this version posted November 18, 2021. The copyright holder for this preprint (which was not certified by peer review) is the author/funder. All rights reserved. No reuse allowed without permission.

dT mispair at position 7 in *TRAC* off-target #2 complex. (**E**) Close-up view of rU-dT pairing at position 9 in *PTPRC*-tgt2 off-target #1 complex, facilitated by base propeller twisting. (**F**) Close-up view of rU-dT pairing at position 8 in *TRAC* off-target #2 complex, enabled by backbone shift of the RNA strand. (**G**) Close-up view of partially paired rC-dC mismatch at position 5 in *AAVS1* off-target #2 complex, bridged by a water molecule. (**H**) Close-up view of rC-dC mispair at position 15 in *AAVS1* off-target #3 complex.

bioRxiv preprint doi: https://doi.org/10.1101/2021.11.18.469088; this version posted November 18, 2021. The copyright holder for this preprint (which was not certified by peer review) is the author/funder. All rights reserved. No reuse allowed without permission.

Figure S9

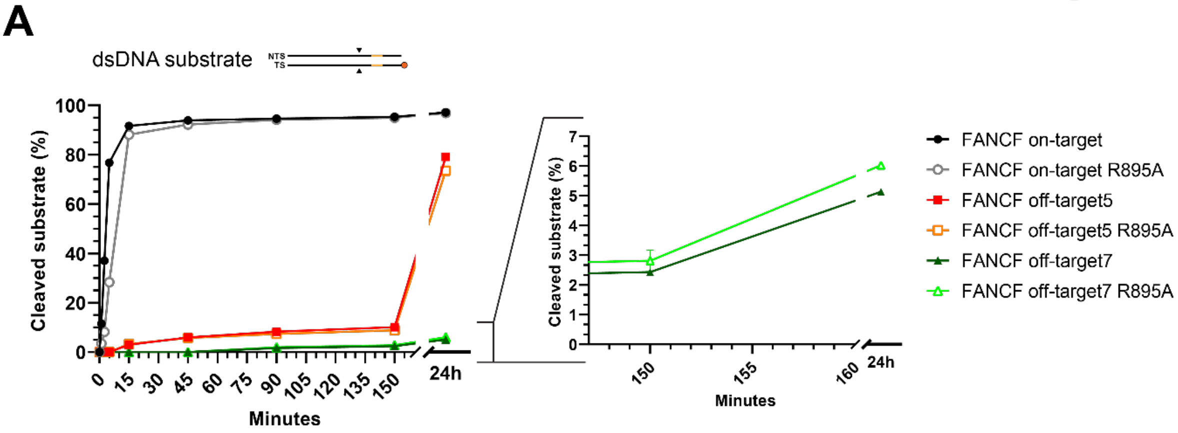

B

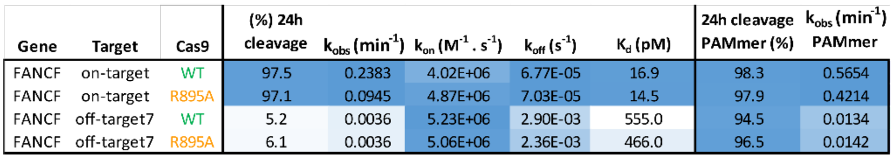

Gene	Target	Cas9	(%) 24h cleavage	k_{obs} (min^{-1})	k_{on} (M^{-1} . s^{-1})	k_{off} (s^{-1})	K_d (pM)	24h cleavage PAMmer (%)	k_{obs} (min^{-1}) PAMmer
FANCF	on-target	WT	97.5	0.2383	4.02E+06	6.77E-05	16.9	98.3	0.5654
FANCF	on-target	R895A	97.1	0.0945	4.87E+06	7.03E-05	14.5	97.9	0.4214
FANCF	off-target7	WT	5.2	0.0036	5.23E+06	2.90E-03	555.0	94.5	0.0134
FANCF	off-target7	R895A	6.1	0.0036	5.06E+06	2.36E-03	466.0	96.5	0.0142

Figure S9. Cas9 **R895A mutation of Cas9 has no significant impact on FANCF off-target #7 cleavage or binding.**

(**A**) Kinetic analysis of *FANCF* on- and off-target substrate DNA cleavage by wild-type and R895A Cas9 proteins. (**B**) Kinetic and thermodynamic parameters of *FANCF* on- and off-target substrate DNA cleavage by wild-type and R895A Cas9. Cleavage rate constants (k_{obs}) were derived from single-exponential function fitting of plots shown in (A). Substrate binding and dissociation rate constants (k_{on} and k_{off}) and the equilibrium dissociation constant (K_d) were determined using a DNA nanolever (switchSENSE) binding assay.

bioRxiv preprint doi: https://doi.org/10.1101/2021.11.18.469088; this version posted November 18, 2021. The copyright holder for this preprint (which was not certified by peer review) is the author/funder. All rights reserved. No reuse allowed without permission.

Figure S10

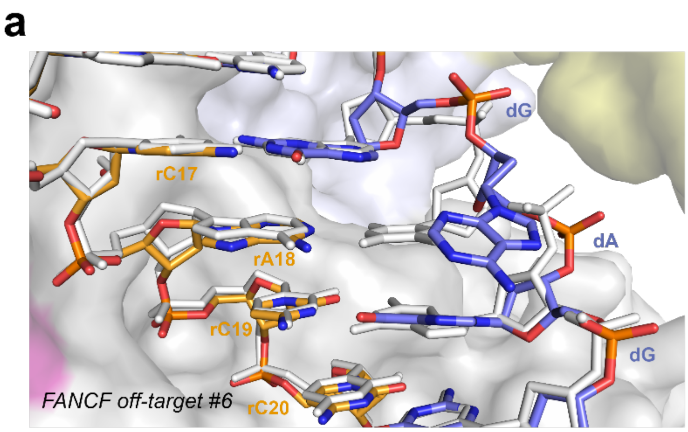

b

	1	2	3	4	5	6	7	8	9	10	11	12	13	14	15	16	17	18	19	20
Total Mismatches	2029	1771	1453	1295	1100	882	888	924	1171	885	632	769	738	409	506	524	484	708	775	801
dA-rA mismatches	139	36	322	74	66	97	72	39	51	85	49	15	7	57	2	24	16	89	155	148
%dA-rA mismatches	10.8%	9.5%	7.8%	6.9%	5.9%	4.7%	4.7%	4.9%	6.3%	4.7%	3.4%	4.1%	3.9%	2.2%	2.7%	2.8%	2.6%	3.8%	4.1%	4.3%

Figure S10. Tolerance of adenine-adenine mismatches within the heteroduplex.

(**A**) Close-up view of rA-dA mismatch at position 18 in *FANCF* off-target #6 complex, overlaid with the *FANCF* on-target structure (white). (**B**) Number of rA-dA off-target mismatches per heteroduplex position recovered in the SITE-Seq assay for all analysed genomic targets. Percentages indicate frequency of rA-dA mismatches recovered in the particular position as a fraction of total number of rA-dA mismatches.

bioRxiv preprint doi: https://doi.org/10.1101/2021.11.18.469088; this version posted November 18, 2021. The copyright holder for this preprint (which was not certified by peer review) is the author/funder. All rights reserved. No reuse allowed without permission.

Figure S11

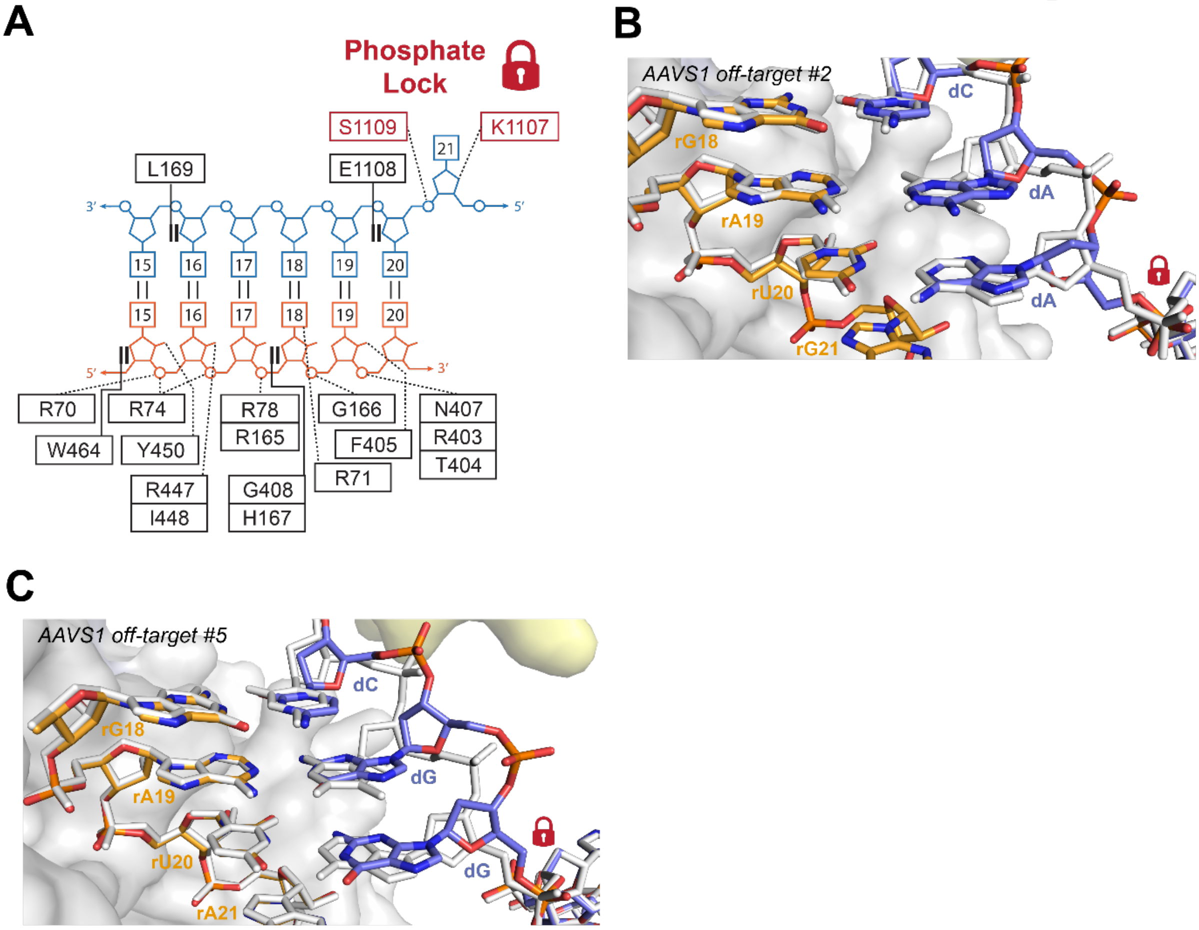

Figure S11. Lack of protein contacts with the target DNA strand in the seed region allows for large phosphate backbone distortions.

(**A**) Schematic overview of Cas9 interactions within the PAM-proximal seed region of the guide RNA-TS DNA heteroduplex. (**B**) Close-up view of the seed region in *AAVS1* off-target #2 complex, overlaid with the AAVS1 on-target heteroduplex (white), showing structural distortion of the TS due to rA-dA mispair at seed position 19. (**C**) Close-up view of the seed region in AAVS1 off-target #5 complex, overlaid with the AAVS1 on-target heteroduplex (white), showing structural distortion due to rA-dG and rU-dG mismatches at positions 19 and 20, respectively. Red lock icon indicates position of the phosphate lock residue in (B) and (C).

bioRxiv preprint doi: https://doi.org/10.1101/2021.11.18.469088; this version posted November 18, 2021. The copyright holder for this preprint (which was not certified by peer review) is the author/funder. All rights reserved. No reuse allowed without permission.

Figure S12

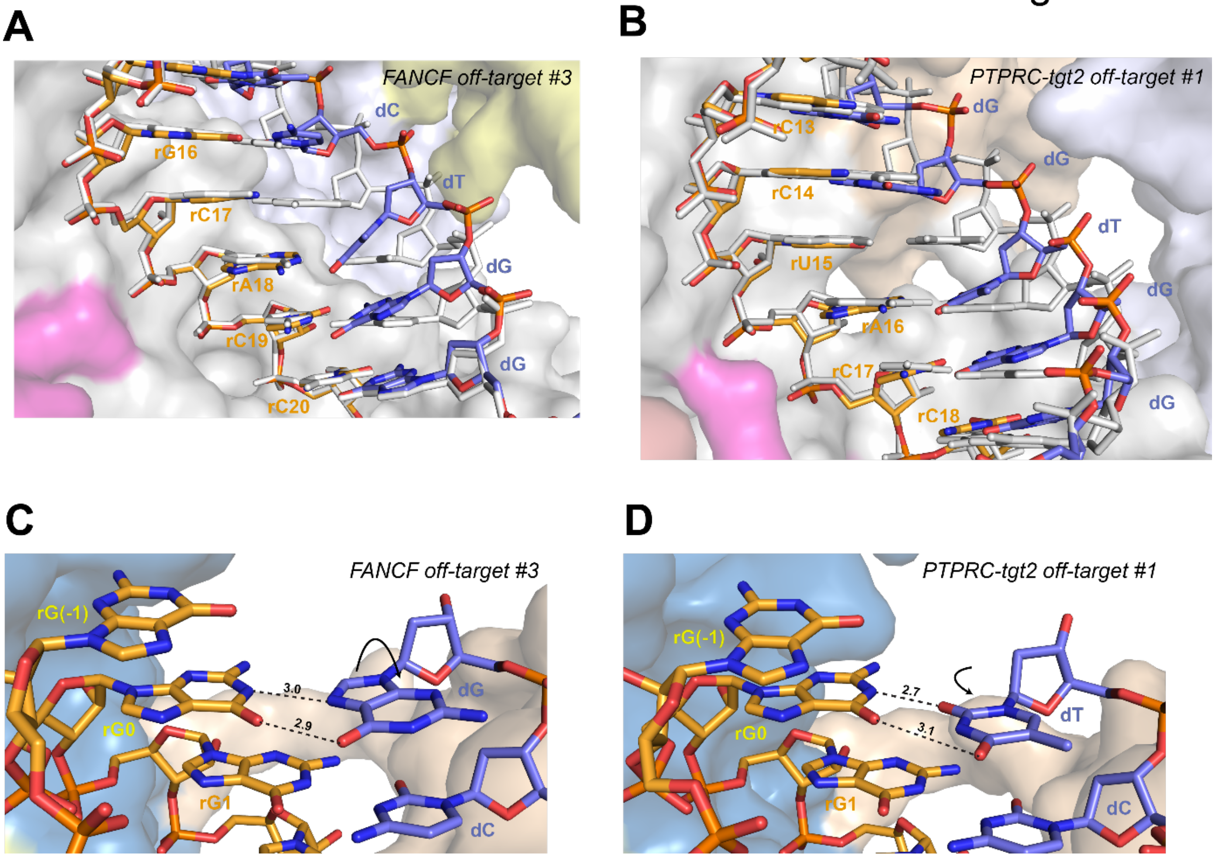

Figure S12. Recognition of off-target sites containing deletions in the seed region.

(**A**) Close-up view of base skipping within the seed region of the guide RNA-off-target DNA heteroduplex in *FANCF* off-target #3 complex, overlaid with the on-target heteroduplex (white). (**B**) Close-up view of base skipping within the seed region of the guide RNA-off-target DNA heteroduplex in *PTPRC-tgt2* off-target #1 complex, overlaid with *FANCF* on-target heteroduplex (white). (**C**) Close-up view of non-canonical base pairs at the 5'-terminus of the guide RNA in *FANCF* off-target #3 complex involving guanosine nucleotides introduced during in vitro transcription of the guide RNA. (**D**) Close-up view of non-canonical base pairs at the 5'-terminus of the guide RNA in *PTPRC-tgt2* off-target #1 complex involving guanosine nucleotides introduced during in vitro transcription of the guide RNA.

bioRxiv preprint doi: https://doi.org/10.1101/2021.11.18.469088; this version posted November 18, 2021. The copyright holder for this preprint (which was not certified by peer review) is the author/funder. All rights reserved. No reuse allowed without permission.

Figure S13

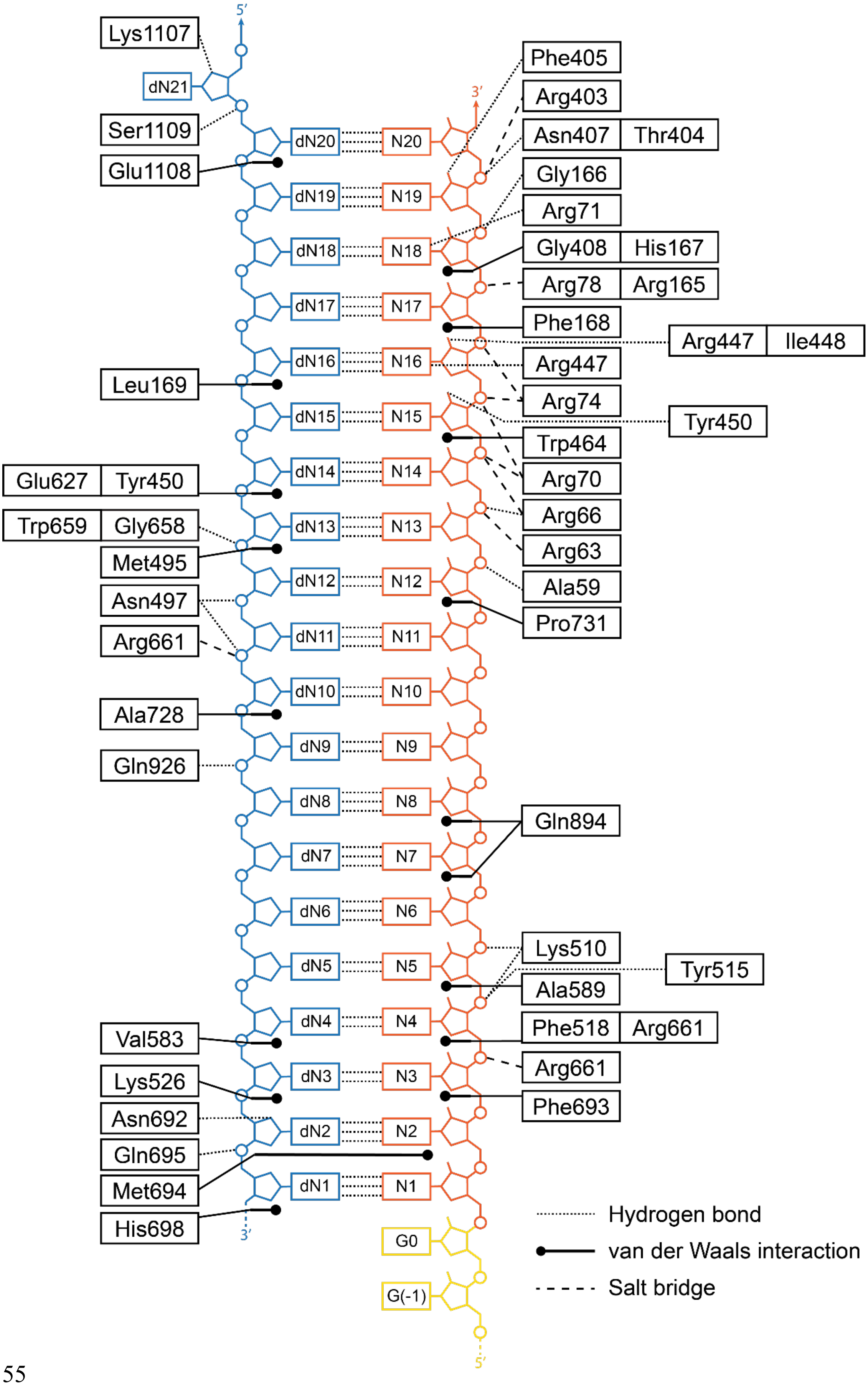

bioRxiv preprint doi: https://doi.org/10.1101/2021.11.18.469088; this version posted November 18, 2021. The copyright holder for this preprint (which was not certified by peer review) is the author/funder. All rights reserved. No reuse allowed without permission.

Figure S13. Cas9-nucleic acid interactions in on-target complexes.

Schematic diagram depicting Cas9 residues interacting with the guide RNA-target DNA heteroduplex. Dotted lines represent hydrogen bonding interactions; dashed lines represent salt bridges; solid lines represent stacking/hydrophobic interactions. Target strand is coloured in blue, guide RNA in orange. Phosphates are represented by circles, ribose moieties by pentagons, and nucleobases by rectangles.

bioRxiv preprint doi: https://doi.org/10.1101/2021.11.18.469088; this version posted November 18, 2021. The copyright holder for this preprint (which was not certified by peer review) is the author/funder. All rights reserved. No reuse allowed without permission.

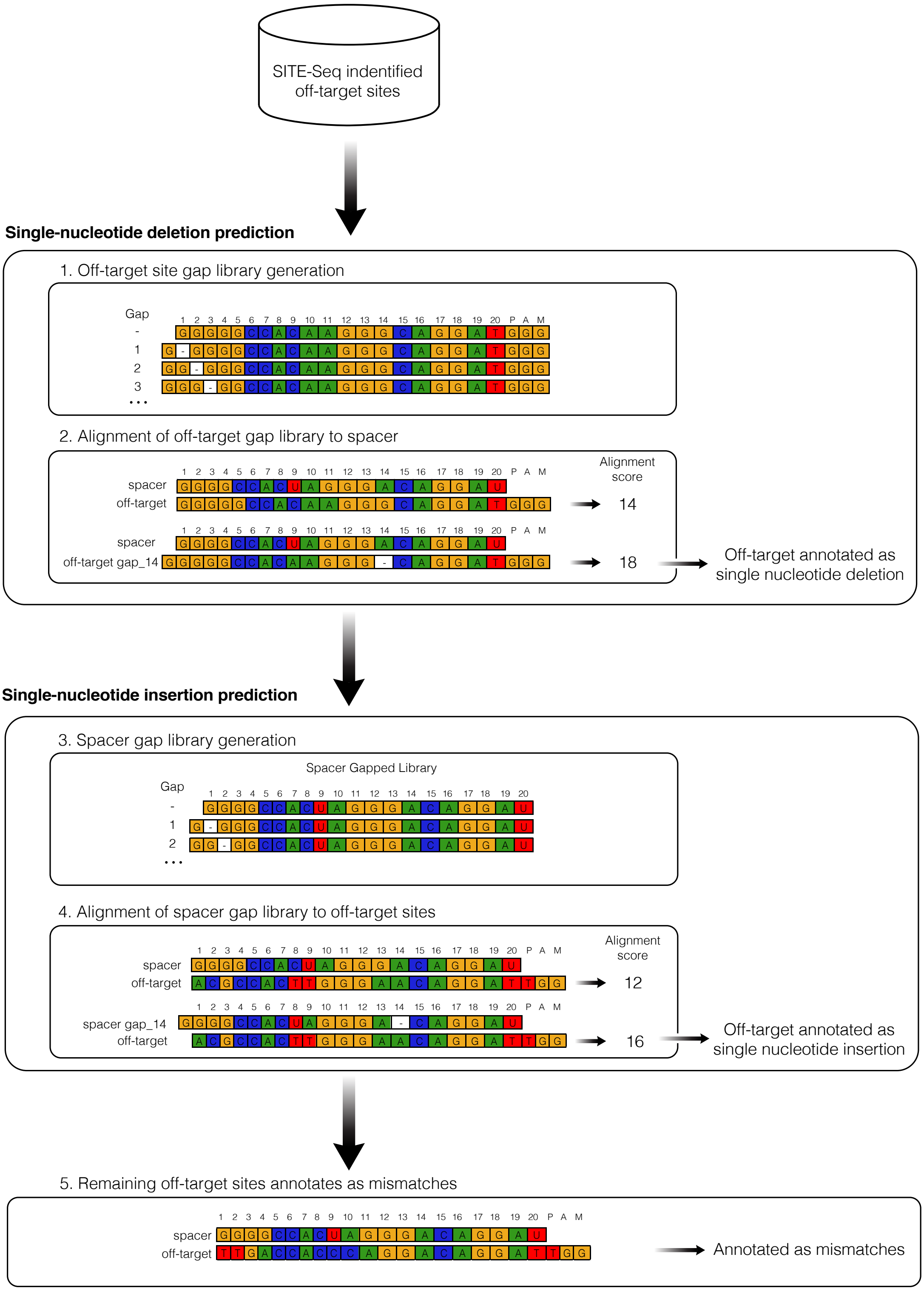
SITE-Seq indentified off-target sites
Single-nucleotide deletion prediction
1. Off-target site gap library generation
Gap
1 2 3 4 5 6 7 8 9 10 11 12 13 14 15 16 17 18 19 20 P A M
- GGGGGCCACAAGGGCAGGATGGG
1 G-GGGGCCACAAGGGCAGGATGGG
2 GG-GGGCCACAAGGGCAGGATGGG
3 GGG-GGCCACAAGGGCAGGATGGG
…
2. Alignment of off-target gap library to spacer
Alignment score
spacer GGGGCCACUAGGGACAGGAU
off-target GGGGGCCACAAGGGCAGGATGGG
14
spacer GGGGCCACUAGGGACAGGAU
off-target gap_14 GGGGGCCACAAGGG-CAGGATGGG
18
Off-target annotated as single nucleotide deletion
Single-nucleotide insertion prediction
3. Spacer gap library generation
Spacer Gapped Library
Gap
- GGGGCCACUAGGGACAGGAU
1 G-GGGCCACUAGGGACAGGAU
2 GG-GGCCACUAGGGACAGGAU
…
4. Alignment of spacer gap library to off-target sites
Alignment score
spacer GGGGCCACUAGGGACAGGAU
off-target ACGCCACTTGGGAACAGGATTGG
12
spacer gap_14 GGGGCCACUAGGGA-CAGGAU
off-target ACGCCACTTGGGAACAGGATTGG
16
Off-target annotated as single nucleotide insertion
5. Remaining off-target sites annotates as mismatches
spacer GGGGCCACUAGGGACAGGAU
off-target TTGACCACCCAGGACAGGATTGG
Annotated as mismatches

Figure S14. Schematic representation of mismatch, insertion, and deletion classification algorithm for the SITE-Seq assay analysis of off-target sites.

bioRxiv preprint doi: https://doi.org/10.1101/2021.11.18.469088; this version posted November 18, 2021. The copyright holder for this preprint (which was not certified by peer review) is the author/funder. All rights reserved. No reuse allowed without permission.

Schematic represents unrestricted classification algorithm of off-target sites with putative insertions and deletions. In the final restricted pipeline, the positioning is limited to heteroduplex positions 6-20 for insertions and positions 10-20 for deletions.

bioRxiv preprint doi: https://doi.org/10.1101/2021.11.18.469088; this version posted November 18, 2021. The copyright holder for this preprint (which was not certified by peer review) is the author/funder. All rights reserved. No reuse allowed without permission.

Figure S15

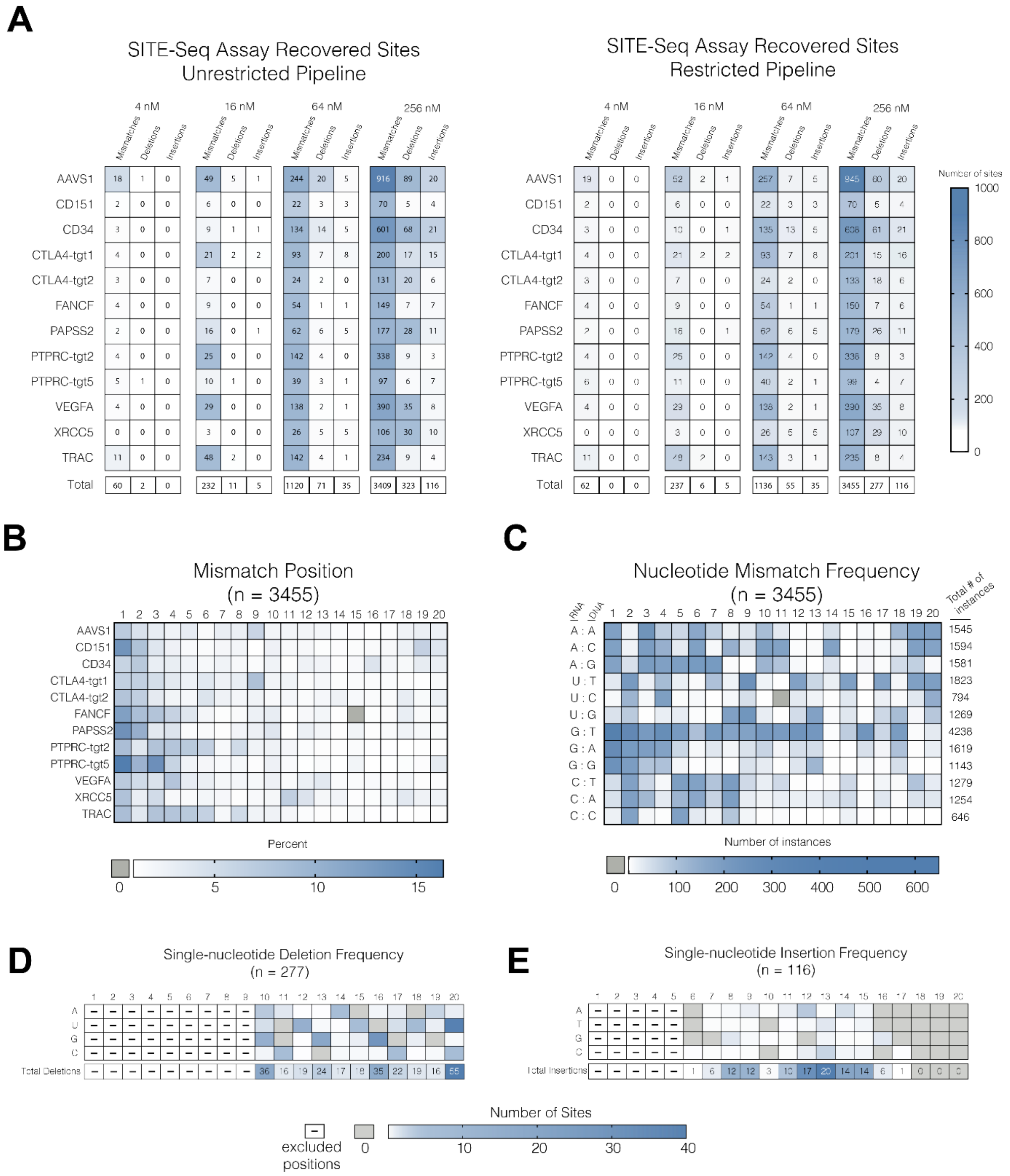

SITE-Seq Assay Recovered Sites — Unrestricted Pipeline

	4 nM			16 nM			64 nM			256 nM		
	Mismatches	Deletions	Insertions	Mismatches	Deletions	Insertions	Mismatches	Deletions	Insertions	Mismatches	Deletions	Insertions
AAVS1	18	1	0	49	5	1	244	20	5	916	89	20
CD151	2	0	0	6	0	0	22	3	3	70	5	4
CD34	3	0	0	9	1	1	134	14	5	601	68	21
CTLA4-tgt1	4	0	0	21	2	2	93	7	8	200	17	15
CTLA4-tgt2	3	0	0	7	0	0	24	2	0	131	20	6
FANCF	4	0	0	9	0	0	54	1	1	149	7	7
PAPSS2	2	0	0	16	0	1	62	6	5	177	28	11
PTPRC-tgt2	4	0	0	25	0	0	142	4	0	338	9	3
PTPRC-tgt5	5	1	0	10	1	0	39	3	1	97	6	7
VEGFA	4	0	0	29	0	0	138	2	1	390	35	8
XRCC5	0	0	0	3	0	0	26	5	5	106	30	10
TRAC	11	0	0	48	2	0	142	4	1	234	9	4
Total	60	2	0	232	11	5	1120	71	35	3409	323	116

SITE-Seq Assay Recovered Sites — Restricted Pipeline

	4 nM			16 nM			64 nM			256 nM		
	Mismatches	Deletions	Insertions	Mismatches	Deletions	Insertions	Mismatches	Deletions	Insertions	Mismatches	Deletions	Insertions
AAVS1	19	0	0	52	2	1	257	7	5	945	60	20
CD151	2	0	0	6	0	0	22	3	3	70	5	4
CD34	3	0	0	10	0	1	135	13	5	608	61	21
CTLA4-tgt1	4	0	0	21	2	2	93	7	8	201	15	16
CTLA4-tgt2	3	0	0	7	0	0	24	2	0	133	18	6
FANCF	4	0	0	9	0	0	54	1	1	150	7	6
PAPSS2	2	0	0	16	0	1	62	6	5	179	26	11
PTPRC-tgt2	4	0	0	25	0	0	142	4	0	338	9	3
PTPRC-tgt5	6	0	0	11	0	0	40	2	1	99	4	7
VEGFA	4	0	0	29	0	0	138	2	1	390	35	8
XRCC5	0	0	0	3	0	0	26	5	5	107	29	10
TRAC	11	0	0	48	2	0	143	3	1	235	8	4
Total	62	0	0	237	6	5	1136	55	35	3455	277	116

Nucleotide Mismatch Frequency — Total # of instances

rRNA : rDNA	Total # of instances
A : A	1545
A : C	1594
A : G	1581
U : T	1823
U : C	794
U : G	1269
G : T	4238
G : A	1619
G : G	1143
C : T	1279
C : A	1254
C : C	646

	1	2	3	4	5	6	7	8	9	10	11	12	13	14	15	16	17	18	19	20
Total Deletions	–	–	–	–	–	–	–	–	–	36	16	19	24	17	18	35	22	19	16	55

	1	2	3	4	5	6	7	8	9	10	11	12	13	14	15	16	17	18	19	20
Total Insertions	–	–	–	–	–	1	6	12	12	3	10	17	20	14	14	6	1	0	0	0

Figure S15. Positional restriction of nucleotide insertions/deletions during of SITE-Seq assay off-target profiling.

(**A**) Number of recovered off-target sites per genomic target as a function of RNP concentration classified as containing either only mismatches, single-nucleotide deletions, or single-nucleotide insertions. Left panel corresponds to classification using algorithm with no

bioRxiv preprint doi: https://doi.org/10.1101/2021.11.18.469088; this version posted November 18, 2021. The copyright holder for this preprint (which was not certified by peer review) is the author/funder. All rights reserved. No reuse allowed without permission.

positional restriction. Right panel corresponds to classification using algorithm restricting deletions to positions 10-20 and insertions to 6-20 only. (**B**) Frequency of positional mismatch occurrence per genomic target for mismatched off-targets with the positionally restricted algorithm. (**C**) Frequency of nucleotide mismatches within the heteroduplex for all off-target sites when classified with a positionally restricted pipeline (n=3445 sites for both (B) and (C)). (**D**) Frequency of single-nucleotide deletions occurring within positions 10-20 of the heteroduplex for all off-target sites when analysed with a positionally restricted pipeline. (n=277 sites). (**E**) Frequency of single-nucleotide insertions occurring within positions 6-20 of the heteroduplex for all off-target sites when analysed with a positionally restricted pipeline. (n=116 sites).

bioRxiv preprint doi: https://doi.org/10.1101/2021.11.18.469088; this version posted November 18, 2021. The copyright holder for this preprint (which was not certified by peer review) is the author/funder. All rights reserved. No reuse allowed without permission.

Figure S16

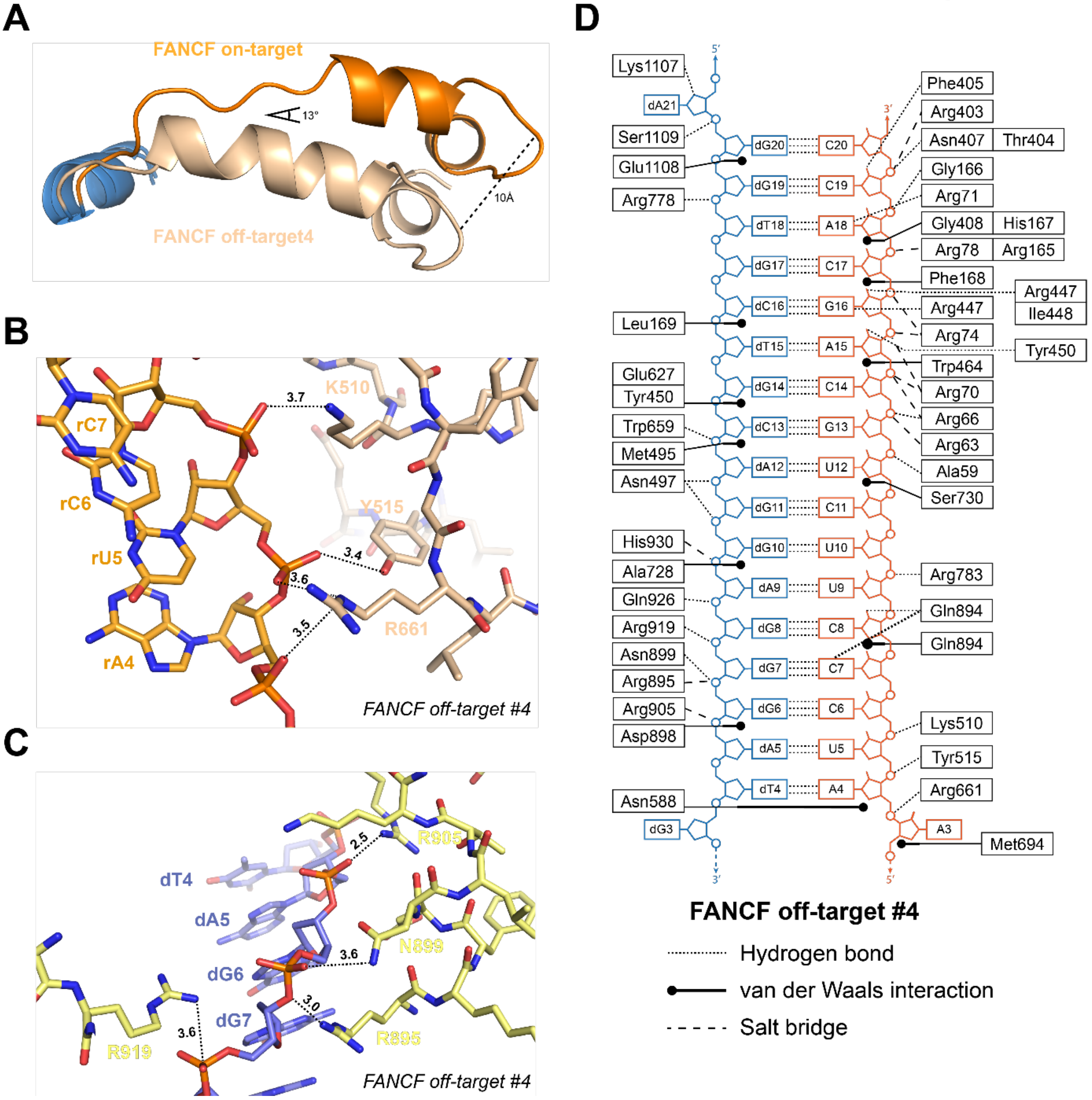

Figure S16. Altered heteroduplex interactions in *FANCF* off-target #4 complex.

(**A**) Overlay of REC3 domain helix 703-712 in *FANCF* off-target #4 complex (wheat) with *FANCF* on-target complex (orange). (**B**) Close-up view of REC3 domain interactions with the guide RNA strand in *FANCF* off-target #4 complex. (**C**) Close-up view of TS DNA interactions established by HNH domain in *FANCF* off-target #4 complex. (**D**) Schematic diagram depicting Cas9 residues interacting with the guide RNA-off-target DNA heteroduplex in *FANCF* off-target #4 complex. Dotted lines represent hydrogen bonding interactions, dashed lines represent salt bridges, solid lines represent stacking/hydrophobic interactions. Target

bioRxiv preprint doi: https://doi.org/10.1101/2021.11.18.469088; this version posted November 18, 2021. The copyright holder for this preprint (which was not certified by peer review) is the author/funder. All rights reserved. No reuse allowed without permission.

strand is coloured blue, guide RNA orange. Phosphates are represented by circles, ribose moieties by pentagons, and nucleobases by rectangles.

bioRxiv preprint doi: https://doi.org/10.1101/2021.11.18.469088; this version posted November 18, 2021. The copyright holder for this preprint (which was not certified by peer review) is the author/funder. All rights reserved. No reuse allowed without permission.

Figure S17

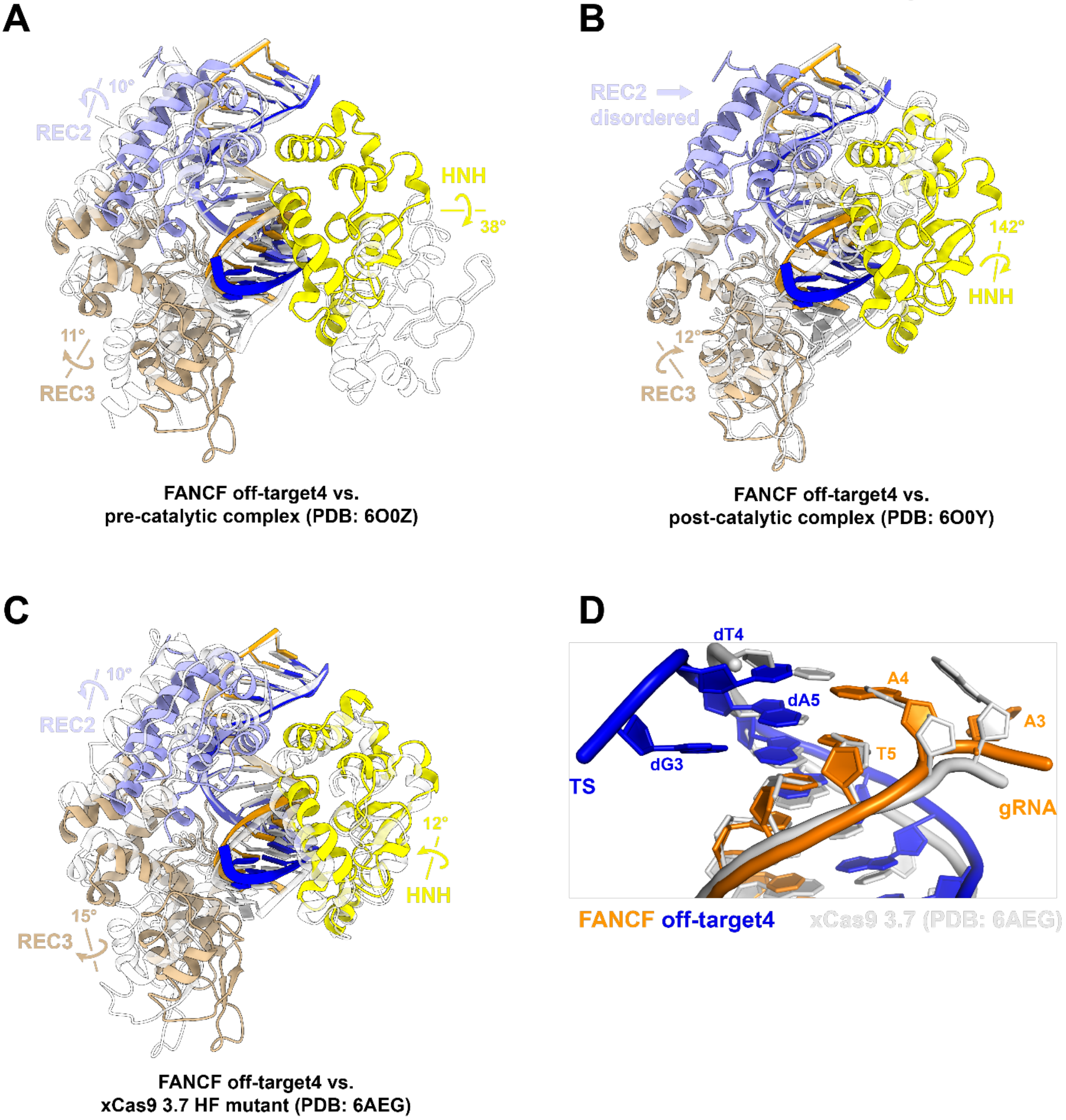

FANCF off-target4 vs.
pre-catalytic complex (PDB: 6O0Z)

FANCF off-target4 vs.
post-catalytic complex (PDB: 6O0Y)

FANCF off-target4 vs.
xCas9 3.7 HF mutant (PDB: 6AEG)

Figure S17. Conformational rearrangements of REC2/3 AND HNH domains in *FANCF* off-target #4 complex.

(**A**) Structural overlay of the *FANCF* off-target #4 complex with cryo-EM structure of a pre-catalytic (State I) Cas9 complex (PDB: 6O0Z). (**B**) Structural overlay of the *FANCF* off-target #4 complex with the cryo-EM structure of a post-catalytic (State II) Cas9 complex (PDB: 6O0Y). (**C**) Structural overlay of the *FANCF* off-target #4 complex with the crystallographic structure of the high-fidelity xCas9 3.7 variant (PDB: 6AEG). The REC1, RuvC, and PAM

bioRxiv preprint doi: https://doi.org/10.1101/2021.11.18.469088; this version posted November 18, 2021. The copyright holder for this preprint (which was not certified by peer review) is the author/funder. All rights reserved. No reuse allowed without permission.

interaction domains have been omitted for clarity in all panels, as no significant structural changes were observed in these domains. The *FANCF* off-target #4 complex domains are colored according to **Figure 1A**. The overlaid structures are coloured white. (**D**) Overlay of the PAM-distal heteroduplex region in *FANCF* off-target #4 and xCas9 3.7 on-target complexes. Target strand is coloured in blue, guide RNA is coloured orange.

bioRxiv preprint doi: https://doi.org/10.1101/2021.11.18.469088; this version posted November 18, 2021. The copyright holder for this preprint (which was not certified by peer review) is the author/funder. All rights reserved. No reuse allowed without permission.

Table S1. SITE-Seq assay results for Cas9 off-target profiling of 12 selected genomic sites. Columns indicate the recovered off-target sequence; motif location; number of substitutions in recovered target sequence compared to the on-target (substitutions); strand designation of PAM; the lowest recovery concentration of each target; and whether the off-target is predicted to contain inserts or deletions based on restricted pipeline paraments. Off-target sites recovered at lower concentrations were also recovered at higher concentrations (e.g., all 4nM sites were also recovered at 16nM, 64 nM, and 256 nM).

Table S2. List of recovered off-target sequences aligned to the corresponding on-target sequence.

Off-target alignments classified by genomic target and by the presence of insertions, deletions or purely mismatched targets, as based on restricted pipeline paraments. Indexes correspond to off-target sequence numbering in Table S1.

Table S3. Crystallographic data collection and refinement statistics of Cas9 on-target and off-target complexes

Table S4. 3DNA 2.0 analysis of the helical parameters and sugar puckering of characterised on-target and off-target duplexes

Table S5. List of oligonucleotides used in this study

bioRxiv preprint doi: https://doi.org/10.1101/2021.11.18.469088; this version posted November 18, 2021. The copyright holder for this preprint (which was not certified by peer review) is the author/funder. All rights reserved. No reuse allowed without permission.

Methods

DNA oligonucleotides and substrates

Sequences of DNA oligonucleotides used in this study are summarised in **Table S5**. Crystallisation substrates were synthesised by Sigma Aldrich without further purification, sgRNA transcription templates and ATTO-532 labelled cleavage substrates were synthesised by Integrated DNA Technologies, Inc., with PAGE and HPLC purification, respectively. Partially double stranded crystallisation substrates were prepared by mixing complementary oligonucleotides in a 1:1 molar ratio (as determined by 260 nm absorption), heating to 95 °C for 5 minutes and slow cooling to room-temperature. Cleavage substrates were prepared similarly, except that a 2-fold molar excess of the non-target strand was used.

Cas9 protein expression and purification

Streptococcus pyogenes Cas9 wild type protein and the nuclease dead mutant (D10A, H840A) were both recombinantly expressed for 16 hours at 18 °C in *Escherichia coli* Rosetta 2 (DE3) (Novagen) N-terminally fused to a hexahistidine affinity tag, the maltose binding protein (MBP) polypeptide, and the tobacco etch virus (TEV) protease cleavage site. Cells were resuspended and lysed in 20 mM HEPES-KOH pH 7.5, 500 mM KCl, 5 mM imidazole, and supplemented with added protease inhibitors. Clarified lysate was loaded on a 10 ml Ni-NTA Superflow column (QIAGEN), washed with 7 column volumes of 20 mM HEPES-KOH pH 7.5, 500 mM KCl, 5 mM imidazole, and eluted with 10 column volumes of 20 mM HEPES-KOH pH 7.5, 250 mM KCl, 200 mM imidazole. Salt concentration is adjusted and protein is loaded on a 10 ml HiTrap Heparin HP column (GE Healthcare) equilibrated in 20 mM HEPES-KOH pH 7.5, 250 mM KCl, 1 mM DTT. The column is washed with 5 column volumes of 20 mM HEPES-KOH pH 7.5, 250 mM KCl, 1 mM DTT, and Cas9 is eluted with 17 column volumes of 20 mM HEPES-KOH pH 7.5, 1.5 M KCl, 1 mM DTT, in a 0-32% gradient (peak elution around 500 mM KCl). His$_6$-MBP tag was removed by TEV protease cleavage overnight

bioRxiv preprint doi: https://doi.org/10.1101/2021.11.18.469088; this version posted November 18, 2021. The copyright holder for this preprint (which was not certified by peer review) is the author/funder. All rights reserved. No reuse allowed without permission.

with gentle shaking. The untagged Cas9 was concentrated and applied to a Superdex 200 16/600 (GE Healthcare) and eluted with 20 mM HEPES-KOH pH 7.5, 500 mM KCl, 1 mM DTT. Purified protein was concentrated to 10 mg/ml, flash frozen in liquid nitrogen and store at -80 °C. DTT was omitted in the size-exclusion step of the purification when protein was used for switchSENSE measurements.

sgRNA transcription and purification

sgRNAs are transcribed from a double stranded PCR product template amplified from a plasmid in a 5 ml transcription reaction (30 mM Tris-HCl pH 8.1, 25 mM $MgCl_2$, 2 mM spermidine, 0.01% Triton X-100, 5 mM CTP, 5 mM ATP, 5 mM GTP, 5 mM UTP, 10 mM DTT, 1 µM DNA transcription template, 0.5 units inorganic pyrophosphatase (Thermo Fischer), 250 µg homemade T7 RNA polymerase. The reaction is incubated at 37 °C for 5 hours, and then treated for 30 minutes with 15 units of RQ1 DNAse (Promega). The transcribed sgRNAs are subsequently PAGE purified on an 8% denaturing (7 M urea) polyacrylamide gel, and lastly ethanol precipitated and resuspended in DEPC treated water.

Crystallisation of Cas9 ternary complexes and structure determination

To assemble the Cas9 on-/off-target ternary complexes, the Cas9 protein is first mixed with the sgRNA in a 1:1.5 molar ratio and incubated at room temperature for 10 minutes. Next, the binary complex is diluted to 2 mg/ml with 20 mM HEPES-KOH 7.5, 250 mM KCl, 1 mM DTT, 2 mM $MgCl_2$ buffer, pre-annealed 100 µM DNA substrate is added in a 1:1.8 molar ratio and the complex is incubated another 10 minutes at room temperature. For crystallisation, 1 µl of the ternary complex (1-2 mg/ml) is mixed with 1 µl of the reservoir solution (0.1 M Tris-acetate pH 8.5, 0.3-0.5 M KSCN, 17-19% PEG3350) and crystals are grown at 20 °C using the hanging drop vapour diffusion method. In some cases, microseeding was be used to improve crystal morphology. Crystals are typically harvested after 2-3 weeks, cryoprotected in 0.1 M Tris-acetate pH 8.5, 0.4 M KSCN, 30% PEG3350, 15% ethylene glycol, 1 mM $MgCl_2$, and flash-

bioRxiv preprint doi: https://doi.org/10.1101/2021.11.18.469088; this version posted November 18, 2021. The copyright holder for this preprint (which was not certified by peer review) is the author/funder. All rights reserved. No reuse allowed without permission.

cooled in liquid nitrogen. Diffraction data was obtained at beamlines PXI and PXIII of the Swiss Light Source (Paul Scherrer Institute, Villigen, Switzerland) and were processed using the XDS package (Kabsch, 2010). Structures were solved by molecular replacement through the Phaser module of the Phenix package (Adams et al., 2010) using the PDB ID: 5FQ5 model omitting the RNA-DNA target duplex from the search. Model adjustment and duplex building was completed using COOT software (Emsley et al., 2010). Atomic model refinement was performed using Phenix.refine (Adams et al., 2010). Protein-nucleic acid interactions were analysed using the PISA web server (Krissinel and Henrick, 2007). Characterisation of the guide-protospacer duplex was performed using the 3DNA 2.0 web server (Li et al., 2019). Structural figures were generated using PyMOL and ChimeraX (Pettersen et al., 2021).

In vitro nuclease activity assays

Cleavage reactions were performed at 37 °C in reaction buffer, containing 20 mM HEPES pH 7.5, 250 mM KCl, 5 mM $MgCl_2$ and 1 mM DTT. First, Cas9 protein was pre-incubated with sgRNA in 1:1.25 ratio for 10 minutes at room temperature. The protein-RNA complex was rapidly mixed with the ATTO-532 labelled dsDNA, to yield final concentrations of 1.67 µM protein and 66.67 nM substrate in a 7.5 µl reaction. Time points were harvested at 1, 2.5, 5, 15, 45, 90, 150 minutes, and 24 hours. Cleavage was stopped by addition of 2 µl of 250 mM EDTA, 0.5% SDS and 20 µg of Proteinase K. Formamide was added to the reactions with final concentration of 50%, samples were incubated at 95 °C for 10 minutes, and resolved on a 15% denaturing PAGE gel containing 7M urea and imaged using a Typhoon FLA 9500 gel imager. Depicted error bars correspond to the standard deviation from four independent cleavage reactions. Rate constants (k_{obs}) were extracted from single exponential fits: [Product] = A*(1-exp(-k_{obs}*t))

switchSENSE analysis

bioRxiv preprint doi: https://doi.org/10.1101/2021.11.18.469088; this version posted November 18, 2021. The copyright holder for this preprint (which was not certified by peer review) is the author/funder. All rights reserved. No reuse allowed without permission.

The target strands (TS) containing a 3' flanking sequence complementary to the ssDNA covalently bound to the chip electrode, and the non-target strands (NTS) (**Table S5**) were resuspended in a buffer containing 10 mM Tris-HCl pH 7.4, 40 mM NaCl, and 0.05% Tween 20. The matching TS:NTS duplex is pre-annealed and hybridised to the chip anode. The Cas9 protein was mixed with the sgRNAs at a 1:2 protein:RNA molar ratio, and the complex was incubated for 30 min at 37 °C in association buffer containing 20 mM HEPES-KOH pH 7.5, 150 mM KCl, 2 mM $MgCl_2$, 0.01% Tween 20. All switchSENSE experiments were performed on a DRX analyser using CAS-48-1-R1-S chips (Dynamic Biosensors GmbH, Martinsried, Germany). Kinetics experiments were performed at 25 °C in association buffer, with an association time of 5 min, dissociation time of 20 min, and a flow rate of 50 µl/min.

SITE-Seq assay

SITE-Seq assay reaction conditions were performed as described previously (Cameron et al., 2017). Briefly, high molecular weight genomic DNA (gDNA) was purified from human primary T cells using the Blood & Cell Culture DNA Maxi Kit (Qiagen) according to the manufacturer's instructions. RNPs comprising the guides were biochemically assembled for gDNA digestion. Specifically, equal molar amounts of crRNA and tracrRNA were mixed and heated to 95 °C for 2 min then allowed to cool at room temperature for ~5 min. Three-fold molar excess of the guides were incubated with *Streptococcus pyogenes* Cas9 (SpCas9) in cleavage reaction buffer (20 mM HEPES pH 7.4, 150 mM KCl, 10 mM MgCl2, 5% glycerol) at 37 °C for 10 min. In a 96-well plate format, 10 µg of gDNA was treated with 0.2 pmol (4 nM), 0.8 pmol (16 nM), 3.2 pmol (64 nM), and 12.8 pmol (256 nM) of each RNP in 50 µL total volume in cleavage reaction buffer. Each cleavage reaction was performed in triplicate. Negative control reactions were assembled in parallel and did not include RNP. gDNA was treated with RNPs for 4 hours at 37 °C. SITE-Seq assay library preparation and sequencing

bioRxiv preprint doi: https://doi.org/10.1101/2021.11.18.469088; this version posted November 18, 2021. The copyright holder for this preprint (which was not certified by peer review) is the author/funder. All rights reserved. No reuse allowed without permission.

was performed as described previously and the final library was loaded onto the Illumina NextSeq platform (Illumina, San Diego, CA), and ~1-3 M reads were obtained for each sample.

SITE-Seq assay analysis and selection for cellular validation

SITE-Seq assay recovered off-targets were filtered for sites that had read-pileups proximal to the expected cut site, a PAM comprising at least one guanine base, fewer than 12 mismatches (reasoning that sites with 12 or more mismatches are likely spurious peaks not resulting from Cas9-induced double-strand breaks), and all sites with 11 mismatches were visually inspected and included in analysis if a putative deletion or insertion would result in a reduction of >4 mismatches relative to the spacer sequence.

In silico mismatch, deletion, and insertion prediction algorithm

Predictive classification of SITE-Seq assay recovered off-target sites as pure mismatches, deletions, or insertions was executed using a scoring algorithm which consisted of the following sequential steps (**Figure S14**):

(i) For each off-target, a gap library was generated where a single nucleotide gap was introduced between each nucleotide in the off-target sequence.

(ii) The off-target gap library was then aligned to the spacer sequence and each alignment was scored based on the number of matched bases between the spacer and gapped off-target pair. If the gapped off-target with the highest alignment score improved alignment by at least 4 nucleotides relative to the non-gapped spacer–off-target alignment, the off-target sequence was marked as a single-nucleotide deletion and removed from subsequent analysis.

(iii) The remaining pool of off-targets were then aligned to a spacer gapped library where a single nucleotide gap was introduced at each positing in the spacer.

(iv) The spacer gap library was then aligned to each off-target sequence and each alignment was scored based on the number of matched bases between the off-target

bioRxiv preprint doi: https://doi.org/10.1101/2021.11.18.469088; this version posted November 18, 2021. The copyright holder for this preprint (which was not certified by peer review) is the author/funder. All rights reserved. No reuse allowed without permission.

and the gapped spacer pair. If the gapped spacer with the highest alignment score improved alignment by at least 4 nucleotides relative to the non-gapped spacer–off-target alignment, the off-target sequence was marked as a single-nucleotide insertion and removed from subsequent analysis.

(v) The remaining off-target for which the spacer–off-target alignment was not improved by single-nucleotide deletions or insertions were annotated as a mismatched off-target.

The prediction pipeline process was the same for the ‘unrestricted’ and structurally-informed ‘restricted’ pipelines, however in the ‘restricted’ pipeline the deletion gap library was restricted to positions 10-20 and the insertion gap library was restricted to positions 6-20.

bioRxiv preprint doi: https://doi.org/10.1101/2021.11.18.469088; this version posted November 18, 2021. The copyright holder for this preprint (which was not certified by peer review) is the author/funder. All rights reserved. No reuse allowed without permission.

References

Abe, N., Dror, I., Yang, L., Slattery, M., Zhou, T., Bussemaker, H.J., Rohs, R., and Mann, R.S. (2015). Deconvolving the recognition of DNA shape from sequence. Cell *161*, 307-318.

Adams, P.D., Afonine, P.V., Bunkoczi, G., Chen, V.B., Davis, I.W., Echols, N., Headd, J.J., Hung, L.W., Kapral, G.J., Grosse-Kunstleve, R.W.*, et al.* (2010). PHENIX: a comprehensive Python-based system for macromolecular structure solution. Acta Crystallogr D Biol Crystallogr *66*, 213-221.

Afek, A., Shi, H., Rangadurai, A., Sahay, H., Senitzki, A., Xhani, S., Fang, M., Salinas, R., Mielko, Z., Pufall, M.A.*, et al.* (2020). DNA mismatches reveal conformational penalties in protein-DNA recognition. Nature.

Anders, C., Niewoehner, O., Duerst, A., and Jinek, M. (2014). Structural basis of PAM-dependent target DNA recognition by the Cas9 endonuclease. Nature *513*, 569-573.

Anzalone, A.V., Koblan, L.W., and Liu, D.R. (2020). Genome editing with CRISPR-Cas nucleases, base editors, transposases and prime editors. Nat Biotechnol *38*, 824-844.

Bae, S., Park, J., and Kim, J.S. (2014). Cas-OFFinder: a fast and versatile algorithm that searches for potential off-target sites of Cas9 RNA-guided endonucleases. Bioinformatics *30*, 1473-1475.

Boyle, E.A., Andreasson, J.O.L., Chircus, L.M., Sternberg, S.H., Wu, M.J., Guegler, C.K., Doudna, J.A., and Greenleaf, W.J. (2017). High-throughput biochemical profiling reveals sequence determinants of dCas9 off-target binding and unbinding. Proc Natl Acad Sci U S A *114*, 5461-5466.

Boyle, E.A., Becker, W.R., Bai, H.B., Chen, J.S., Doudna, J.A., and Greenleaf, W.J. (2021). Quantification of Cas9 binding and cleavage across diverse guide sequences maps landscapes of target engagement. Science Advances *7*, eabe5496.

Bravo, J.P.K., Liu, M.-S., McCool, R.S., Jung, K., Johnson, K.A., and Taylor, D.W. (2021). Structural basis for mismatch surveillance by CRISPR/Cas9. bioRxiv, 2021.2009.2014.460224.

Cameron, P., Fuller, C.K., Donohoue, P.D., Jones, B.N., Thompson, M.S., Carter, M.M., Gradia, S., Vidal, B., Garner, E., Slorach, E.M.*, et al.* (2017). Mapping the genomic landscape of CRISPR-Cas9 cleavage. Nat Methods *14*, 600-606.

Chen, J.S., Dagdas, Y.S., Kleinstiver, B.P., Welch, M.M., Sousa, A.A., Harrington, L.B., Sternberg, S.H., Joung, J.K., Yildiz, A., and Doudna, J.A. (2017). Enhanced proofreading governs CRISPR-Cas9 targeting accuracy. Nature *550*, 407-410.

Cofsky, J.C., Soczek, K.M., Knott, G.J., Nogales, E., and Doudna, J.A. (2021). CRISPR-Cas9 bends and twists DNA to read its sequence. bioRxiv, 2021.2009.2006.459219.

Dagdas, Y.S., Chen, J.S., Sternberg, S.H., Doudna, J.A., and Yildiz, A. (2017). A conformational checkpoint between DNA binding and cleavage by CRISPR-Cas9. Sci Adv *3*, eaao0027.

Deltcheva, E., Chylinski, K., Sharma, C.M., Gonzales, K., Chao, Y., Pirzada, Z.A., Eckert, M.R., Vogel, J., and Charpentier, E. (2011). CRISPR RNA maturation by trans-encoded small RNA and host factor RNase III. Nature *471*, 602-607.

Deveau, H., Barrangou, R., Garneau, J.E., Labonte, J., Fremaux, C., Boyaval, P., Romero, D.A., Horvath, P., and Moineau, S. (2008). Phage response to CRISPR-encoded resistance in Streptococcus thermophilus. J Bacteriol *190*, 1390-1400.

Doench, J.G., Fusi, N., Sullender, M., Hegde, M., Vaimberg, E.W., Donovan, K.F., Smith, I., Tothova, Z., Wilen, C., Orchard, R.*, et al.* (2016). Optimized sgRNA design to maximize activity and minimize off-target effects of CRISPR-Cas9. Nat Biotechnol *34*, 184-191.

bioRxiv preprint doi: https://doi.org/10.1101/2021.11.18.469088; this version posted November 18, 2021. The copyright holder for this preprint (which was not certified by peer review) is the author/funder. All rights reserved. No reuse allowed without permission.

Donohoue, P.D., Pacesa, M., Lau, E., Vidal, B., Irby, M.J., Nyer, D.B., Rotstein, T., Banh, L., Toh, M.S., Gibson, J., *et al.* (2021). Conformational control of Cas9 by CRISPR hybrid RNA-DNA guides mitigates off-target activity in T cells. Mol Cell *81*, 3637-3649 e3635.

Emsley, P., Lohkamp, B., Scott, W.G., and Cowtan, K. (2010). Features and development of Coot. Acta Crystallogr D Biol Crystallogr *66*, 486-501.

Fu, B.X.H., Smith, J.D., Fuchs, R.T., Mabuchi, M., Curcuru, J., Robb, G.B., and Fire, A.Z. (2019). Target-dependent nickase activities of the CRISPR-Cas nucleases Cpf1 and Cas9. Nat Microbiol *4*, 888-897.

Fu, Y., Sander, J.D., Reyon, D., Cascio, V.M., and Joung, J.K. (2014). Improving CRISPR-Cas nuclease specificity using truncated guide RNAs. Nat Biotechnol *32*, 279-284.

Garg, A., and Heinemann, U. (2018). A novel form of RNA double helix based on G.U and C.A(+) wobble base pairing. RNA *24*, 209-218.

Gong, S., Yu, H.H., Johnson, K.A., and Taylor, D.W. (2018). DNA Unwinding Is the Primary Determinant of CRISPR-Cas9 Activity. Cell Rep *22*, 359-371.

Guo, M., Ren, K., Zhu, Y., Tang, Z., Wang, Y., Zhang, B., and Huang, Z. (2019). Structural insights into a high fidelity variant of SpCas9. Cell Res *29*, 183-192.

Hsu, P.D., Scott, D.A., Weinstein, J.A., Ran, F.A., Konermann, S., Agarwala, V., Li, Y., Fine, E.J., Wu, X., Shalem, O., *et al.* (2013). DNA targeting specificity of RNA-guided Cas9 nucleases. Nat Biotechnol *31*, 827-832.

Ivanov, I.E., Wright, A.V., Cofsky, J.C., Aris, K.D.P., Doudna, J.A., and Bryant, Z. (2020). Cas9 interrogates DNA in discrete steps modulated by mismatches and supercoiling. Proc Natl Acad Sci U S A *117*, 5853-5860.

Jiang, F., Taylor, D.W., Chen, J.S., Kornfeld, J.E., Zhou, K., Thompson, A.J., Nogales, E., and Doudna, J.A. (2016). Structures of a CRISPR-Cas9 R-loop complex primed for DNA cleavage. Science *351*, 867-871.

Jiang, F., Zhou, K., Ma, L., Gressel, S., and Doudna, J.A. (2015). STRUCTURAL BIOLOGY. A Cas9-guide RNA complex preorganized for target DNA recognition. Science *348*, 1477-1481.

Jinek, M., Chylinski, K., Fonfara, I., Hauer, M., Doudna, J.A., and Charpentier, E. (2012). A programmable dual-RNA-guided DNA endonuclease in adaptive bacterial immunity. Science *337*, 816-821.

Jones, S.K., Jr., Hawkins, J.A., Johnson, N.V., Jung, C., Hu, K., Rybarski, J.R., Chen, J.S., Doudna, J.A., Press, W.H., and Finkelstein, I.J. (2020). Massively parallel kinetic profiling of natural and engineered CRISPR nucleases. Nat Biotechnol.

Kabsch, W. (2010). Xds. Acta Crystallogr D Biol Crystallogr *66*, 125-132.

Kimsey, I.J., Petzold, K., Sathyamoorthy, B., Stein, Z.W., and Al-Hashimi, H.M. (2015). Visualizing transient Watson-Crick-like mispairs in DNA and RNA duplexes. Nature *519*, 315-320.

Kimsey, I.J., Szymanski, E.S., Zahurancik, W.J., Shakya, A., Xue, Y., Chu, C.C., Sathyamoorthy, B., Suo, Z., and Al-Hashimi, H.M. (2018). Dynamic basis for dG*dT misincorporation via tautomerization and ionization. Nature *554*, 195-201.

Kitayner, M., Rozenberg, H., Rohs, R., Suad, O., Rabinovich, D., Honig, B., and Shakked, Z. (2010). Diversity in DNA recognition by p53 revealed by crystal structures with Hoogsteen base pairs. Nat Struct Mol Biol *17*, 423-429.

Krissinel, E., and Henrick, K. (2007). Inference of macromolecular assemblies from crystalline state. J Mol Biol *372*, 774-797.

bioRxiv preprint doi: https://doi.org/10.1101/2021.11.18.469088; this version posted November 18, 2021. The copyright holder for this preprint (which was not certified by peer review) is the author/funder. All rights reserved. No reuse allowed without permission.

Kulcsar, P.I., Talas, A., Toth, E., Nyeste, A., Ligeti, Z., Welker, Z., and Welker, E. (2020). Blackjack mutations improve the on-target activities of increased fidelity variants of SpCas9 with 5'G-extended sgRNAs. Nat Commun *11*, 1223.

Kunkel, T.A., and Bebenek, K. (2000). DNA replication fidelity. Annu Rev Biochem *69*, 497-529.

Kuscu, C., Arslan, S., Singh, R., Thorpe, J., and Adli, M. (2014). Genome-wide analysis reveals characteristics of off-target sites bound by the Cas9 endonuclease. Nat Biotechnol *32*, 677-683.

Lazzarotto, C.R., Malinin, N.L., Li, Y., Zhang, R., Yang, Y., Lee, G., Cowley, E., He, Y., Lan, X., Jividen, K., *et al.* (2020). CHANGE-seq reveals genetic and epigenetic effects on CRISPR-Cas9 genome-wide activity. Nat Biotechnol.

Leontis, N.B., Stombaugh, J., and Westhof, E. (2002). The non-Watson-Crick base pairs and their associated isostericity matrices. Nucleic Acids Res *30*, 3497-3531.

Li, S., Olson, W.K., and Lu, X.J. (2019). Web 3DNA 2.0 for the analysis, visualization, and modeling of 3D nucleic acid structures. Nucleic Acids Res *47*, W26-W34.

Lin, Y., Cradick, T.J., Brown, M.T., Deshmukh, H., Ranjan, P., Sarode, N., Wile, B.M., Vertino, P.M., Stewart, F.J., and Bao, G. (2014). CRISPR/Cas9 systems have off-target activity with insertions or deletions between target DNA and guide RNA sequences. Nucleic Acids Res *42*, 7473-7485.

Makarova, K.S., Wolf, Y.I., Iranzo, J., Shmakov, S.A., Alkhnbashi, O.S., Brouns, S.J.J., Charpentier, E., Cheng, D., Haft, D.H., Horvath, P., *et al.* (2020). Evolutionary classification of CRISPR-Cas systems: a burst of class 2 and derived variants. Nat Rev Microbiol *18*, 67-83.

Mekler, V., Minakhin, L., and Severinov, K. (2017). Mechanism of duplex DNA destabilization by RNA-guided Cas9 nuclease during target interrogation. Proc Natl Acad Sci U S A *114*, 5443-5448.

Mitchell, B.P., Hsu, R.V., Medrano, M.A., Zewde, N.T., Narkhede, Y.B., and Palermo, G. (2020). Spontaneous Embedding of DNA Mismatches Within the RNA:DNA Hybrid of CRISPR-Cas9. Frontiers in Molecular Biosciences *7*.

Mullally, G., van Aelst, K., Naqvi, M.M., Diffin, F.M., Karvelis, T., Gasiunas, G., Siksnys, V., and Szczelkun, M.D. (2020). 5' modifications to CRISPR-Cas9 gRNA can change the dynamics and size of R-loops and inhibit DNA cleavage. Nucleic Acids Res.

Murugan, K., Seetharam, A.S., Severin, A.J., and Sashital, D.G. (2020). High-throughput <em>in vitro</em> specificity profiling of natural and high-fidelity CRISPR-Cas9 variants. bioRxiv, 2020.2005.2012.091991.

Nishimasu, H., Ran, F.A., Hsu, P.D., Konermann, S., Shehata, S.I., Dohmae, N., Ishitani, R., Zhang, F., and Nureki, O. (2014). Crystal structure of Cas9 in complex with guide RNA and target DNA. Cell *156*, 935-949.

O'Connell, M.R., Oakes, B.L., Sternberg, S.H., East-Seletsky, A., Kaplan, M., and Doudna, J.A. (2014). Programmable RNA recognition and cleavage by CRISPR/Cas9. Nature *516*, 263-266.

O'Geen, H., Henry, I.M., Bhakta, M.S., Meckler, J.F., and Segal, D.J. (2015). A genome-wide analysis of Cas9 binding specificity using ChIP-seq and targeted sequence capture. Nucleic Acids Res *43*, 3389-3404.

Okafor, I.C., Singh, D., Wang, Y., Jung, M., Wang, H., Mallon, J., Bailey, S., Lee, J.K., and Ha, T. (2019). Single molecule analysis of effects of non-canonical guide RNAs and specificity-enhancing mutations on Cas9-induced DNA unwinding. Nucleic Acids Res *47*, 11880-11888.

Pacesa, M., and Jinek, M. (2021). Mechanism of R-loop formation and conformational activation of Cas9. bioRxiv, 2021.2009.2016.460614.

bioRxiv preprint doi: https://doi.org/10.1101/2021.11.18.469088; this version posted November 18, 2021. The copyright holder for this preprint (which was not certified by peer review) is the author/funder. All rights reserved. No reuse allowed without permission.

Palermo, G., Chen, J.S., Ricci, C.G., Rivalta, I., Jinek, M., Batista, V.S., Doudna, J.A., and McCammon, J.A. (2018). Key role of the REC lobe during CRISPR-Cas9 activation by 'sensing', 'regulating', and 'locking' the catalytic HNH domain. Q Rev Biophys *51*.

Pattanayak, V., Lin, S., Guilinger, J.P., Ma, E., Doudna, J.A., and Liu, D.R. (2013). High-throughput profiling of off-target DNA cleavage reveals RNA-programmed Cas9 nuclease specificity. Nat Biotechnol *31*, 839-843.

Pettersen, E.F., Goddard, T.D., Huang, C.C., Meng, E.C., Couch, G.S., Croll, T.I., Morris, J.H., and Ferrin, T.E. (2021). UCSF ChimeraX: Structure visualization for researchers, educators, and developers. Protein Sci *30*, 70-82.

Ricci, C.G., Chen, J.S., Miao, Y., Jinek, M., Doudna, J.A., McCammon, J.A., and Palermo, G. (2019). Deciphering Off-Target Effects in CRISPR-Cas9 through Accelerated Molecular Dynamics. ACS Cent Sci *5*, 651-662.

Rodnina, M.V., and Wintermeyer, W. (2001). Fidelity of aminoacyl-tRNA selection on the ribosome: kinetic and structural mechanisms. Annu Rev Biochem *70*, 415-435.

Rohs, R., West, S.M., Liu, P., and Honig, B. (2009a). Nuance in the double-helix and its role in protein-DNA recognition. Curr Opin Struct Biol *19*, 171-177.

Rohs, R., West, S.M., Sosinsky, A., Liu, P., Mann, R.S., and Honig, B. (2009b). The role of DNA shape in protein-DNA recognition. Nature *461*, 1248-1253.

Semenova, E., Jore, M.M., Datsenko, K.A., Semenova, A., Westra, E.R., Wanner, B., van der Oost, J., Brouns, S.J., and Severinov, K. (2011). Interference by clustered regularly interspaced short palindromic repeat (CRISPR) RNA is governed by a seed sequence. Proc Natl Acad Sci U S A *108*, 10098-10103.

Singh, D., Sternberg, S.H., Fei, J., Doudna, J.A., and Ha, T. (2016). Real-time observation of DNA recognition and rejection by the RNA-guided endonuclease Cas9. Nat Commun *7*, 12778.

Stemmer, M., Thumberger, T., Del Sol Keyer, M., Wittbrodt, J., and Mateo, J.L. (2015). CCTop: An Intuitive, Flexible and Reliable CRISPR/Cas9 Target Prediction Tool. PLoS One *10*, e0124633.

Sternberg, S.H., LaFrance, B., Kaplan, M., and Doudna, J.A. (2015). Conformational control of DNA target cleavage by CRISPR-Cas9. Nature *527*, 110-113.

Sternberg, S.H., Redding, S., Jinek, M., Greene, E.C., and Doudna, J.A. (2014). DNA interrogation by the CRISPR RNA-guided endonuclease Cas9. Nature *507*, 62-67.

Timsit, Y. (1999). DNA structure and polymerase fidelity. J Mol Biol *293*, 835-853.

Tsai, S.Q., Nguyen, N.T., Malagon-Lopez, J., Topkar, V.V., Aryee, M.J., and Joung, J.K. (2017). CIRCLE-seq: a highly sensitive in vitro screen for genome-wide CRISPR-Cas9 nuclease off-targets. Nat Methods *14*, 607-614.

Tsai, S.Q., Zheng, Z., Nguyen, N.T., Liebers, M., Topkar, V.V., Thapar, V., Wyvekens, N., Khayter, C., Iafrate, A.J., Le, L.P., *et al.* (2015). GUIDE-seq enables genome-wide profiling of off-target cleavage by CRISPR-Cas nucleases. Nat Biotechnol *33*, 187-197.

van Houte, S., Ekroth, A.K., Broniewski, J.M., Chabas, H., Ashby, B., Bondy-Denomy, J., Gandon, S., Boots, M., Paterson, S., Buckling, A., *et al.* (2016). The diversity-generating benefits of a prokaryotic adaptive immune system. Nature *532*, 385-388.

Vlot, M., Houkes, J., Lochs, S.J.A., Swarts, D.C., Zheng, P., Kunne, T., Mohanraju, P., Anders, C., Jinek, M., van der Oost, J., *et al.* (2018). Bacteriophage DNA glucosylation impairs target DNA binding by type I and II but not by type V CRISPR-Cas effector complexes. Nucleic Acids Res *46*, 873-885.

Wang, W., Hellinga, H.W., and Beese, L.S. (2011). Structural evidence for the rare tautomer hypothesis of spontaneous mutagenesis. Proc Natl Acad Sci U S A *108*, 17644-17648.

Wu, X., Scott, D.A., Kriz, A.J., Chiu, A.C., Hsu, P.D., Dadon, D.B., Cheng, A.W., Trevino, A.E., Konermann, S., Chen, S., *et al.* (2014). Genome-wide binding of the CRISPR endonuclease Cas9 in mammalian cells. Nat Biotechnol *32*, 670-676.

bioRxiv preprint doi: https://doi.org/10.1101/2021.11.18.469088; this version posted November 18, 2021. The copyright holder for this preprint (which was not certified by peer review) is the author/funder. All rights reserved. No reuse allowed without permission.

Yakovchuk, P., Protozanova, E., and Frank-Kamenetskii, M.D. (2006). Base-stacking and base-pairing contributions into thermal stability of the DNA double helix. Nucleic Acids Res *34*, 564-574.

Yang, M., Peng, S., Sun, R., Lin, J., Wang, N., and Chen, C. (2018). The Conformational Dynamics of Cas9 Governing DNA Cleavage Are Revealed by Single-Molecule FRET. Cell Rep *22*, 372-382.

Yaung, S.J., Esvelt, K.M., and Church, G.M. (2014). CRISPR/Cas9-mediated phage resistance is not impeded by the DNA modifications of phage T4. PLoS One *9*, e98811.

Zeng, Y., Cui, Y., Zhang, Y., Zhang, Y., Liang, M., Chen, H., Lan, J., Song, G., and Lou, J. (2018). The initiation, propagation and dynamics of CRISPR-SpyCas9 R-loop complex. Nucleic Acids Res *46*, 350-361.

Zhang, L., Rube, H.T., Vakulskas, C.A., Behlke, M.A., Bussemaker, H.J., and Pufall, M.A. (2020). Systematic in vitro profiling of off-target affinity, cleavage and efficiency for CRISPR enzymes. Nucleic Acids Research.

Zhu, X., Clarke, R., Puppala, A.K., Chittori, S., Merk, A., Merrill, B.J., Simonovic, M., and Subramaniam, S. (2019). Cryo-EM structures reveal coordinated domain motions that govern DNA cleavage by Cas9. Nat Struct Mol Biol *26*, 679-685.